JOURNAL OF GEOPHYSICAL RESEARCH, VOL. 97, NO. B4, PAGES 4865–4883, APRIL 10, 1992

Seismicity and Geometry of a 110-km-Long Blind Thrust Fault 2. Synthesis of the 1982–1985 California Earthquake Sequence

ROSS S. STEIN

U.S. Geological Survey, Menlo Park, California

GORAN EKSTROM

Department of Earth and Planetary Sciences, Harvard University, Cambridge, Massachusetts

During 1982–1985, three $5.4 \leq M_w \leq 6.5$ earthquakes migrated 65 km along the north half of a string of Quaternary folds at the east front of the California Coast Ranges. There is no surface fault associated with these earthquakes, but the fold chain, oriented parallel to the San Andreas fault 30 km to the west, takes up contraction normal to the San Andreas fault. Identification of active blind thrust faults is hindered by the absence of a fault trace but may be revealed by the presence of growing folds at the surface and by earthquakes at depth. Because of excellent seismic, geodetic, and geologic data, this earthquake sequence illuminates the geometry of the blind faults and enables us to probe their mechanics. We relocate seismicity and compute focal mechanisms in a three-dimensional velocity space and model the vertical deformation associated with the 1983 **M** = 6.5 Coalinga earthquake. The aftershock zones abut at echelon offsets in the fold axes, and the mainshocks display reverse slip perpendicular to the axes, suggesting that the folds conceal a contiguous, segmented thrust fault. Background seismicity concentrates at bends and breaks in the fold chain, sites that may correspond to tears and ramps in the thrust fault at depth. Seismic reflection profiles reveal thrust and reverse faults dipping toward the San Andreas fault at depths of 5–10 km with several kilometers of cumulative slip and high-angle reverse faults in the anticlines with several hundred meters cumulative slip. Coseismic fold uplift accompanied the Coalinga and Kettleman Hills North Dome earthquakes, suggesting that fold growth is episodic and coupled closely to repeated earthquakes on the underlying thrusts. The north half of the fold chain has been the site of several $6 \leq \mathbf{M} \leq 6.5$ earthquakes since 1885. Thus Kettleman Hills Middle Dome, the next fold segment to the south, has an elevated seismic potential. The aftershock zones of the three main shocks are diffuse and occupy a region much larger than the site of seismic slip. Aftershocks occur 5–7 km from the fault, regions where, on the basis of a boundary element model, the shear strain increase caused by the fault slip exceeds ~20 ppm (equivalent to about 0.7 MPa). We argue that the broad aftershock zone is a product of high, sustained off-fault stress caused by repeated displacement on faults that do not cut the Earth's surface. The fault tip stresses lead to the formation of secondary faults, which can become sites of aftershocks and postseismic creep.

INTRODUCTION

The regular progression of the 1982 **M** = 5.5 New Idria, the 1983 **M** = 6.5 Coalinga, and the 1985 **M** = 6.1 Kettleman Hills North Dome earthquakes is comparable to sequences along major plate boundary faults, such as the 1939–1944 earthquakes along the North Anatolian fault [*Richter*, 1958], except that in the California sequence the aftershock zones abut at en echelon offsets of surface fold axes, rather than at offsets of the faults. These observations motivate the hypothesis that the 110-km-long string of folds beneath which the earthquakes occurred masks a continuous, yet segmented fault that does not reach the Earth's surface, or, in the parlance of petroleum geologists, is "blind."

The 1982–1985 sequence took place along the east margin of the California Coast Ranges. The Coast Ranges appear to be the product of the obliquity of the Pacific–North American plate motion vector to the San Andreas fault. At the 36°N latitude of the Idria–Lost Hills fold belt, the San Andreas fault is oriented 5° ± 2° counterclockwise to the direction of plate motion predicted by NUVEL 1 [*DeMets et al.*, 1990] and displays a Quaternary and contemporary slip rate of 35 mm yr^{-1} [*Sieh and Jahns*, 1984], whereas the plate motion rate is 48 ± 1 mm yr^{-1}. The discrepancy between the plate motion vector and the combined San Andreas fault slip and Basin and Range opening can be resolved into components parallel and perpendicular to the San Andreas fault: The parallel component is 4 ± 1 mm yr^{-1} of right-lateral motion, and the perpendicular component is 7 ± 1.5 mm yr^{-1} of contraction. We estimate the mean slip rate on the thrust beneath the fold chain to be 1–2 mm yr^{-1}.

Ekström et al. [this issue] (hereinafter referred to as paper 1) studied the seismicity, geodesy, and geologic structure of the 1985 Kettleman Hills North Dome earthquake. Here we examine the earthquakes at New Idria and Coalinga and synthesize what we have learned about the entire sequence and the fault on which they occurred. We recalculate the earthquake hypocenters and focal mechanisms for larger events within the region circumscribing the fold chain, relocate seismicity recorded by the northern California seismic network (Calnet) since 1969, and reexamine the historical earthquake record. In addition, we perform numerical experiments to study the fault slip and geometry using the geodetic deformation associated with the 1983 Coalinga earthquake, expanding on previous work [*Stein and King*, 1984; *Stein and Yeats*, 1989] with an augmented data set and new analytical tools. Finally, we assemble seismic reflection

Paper number 91JB02847.
0148-0227/92/91JB-02847$05.00

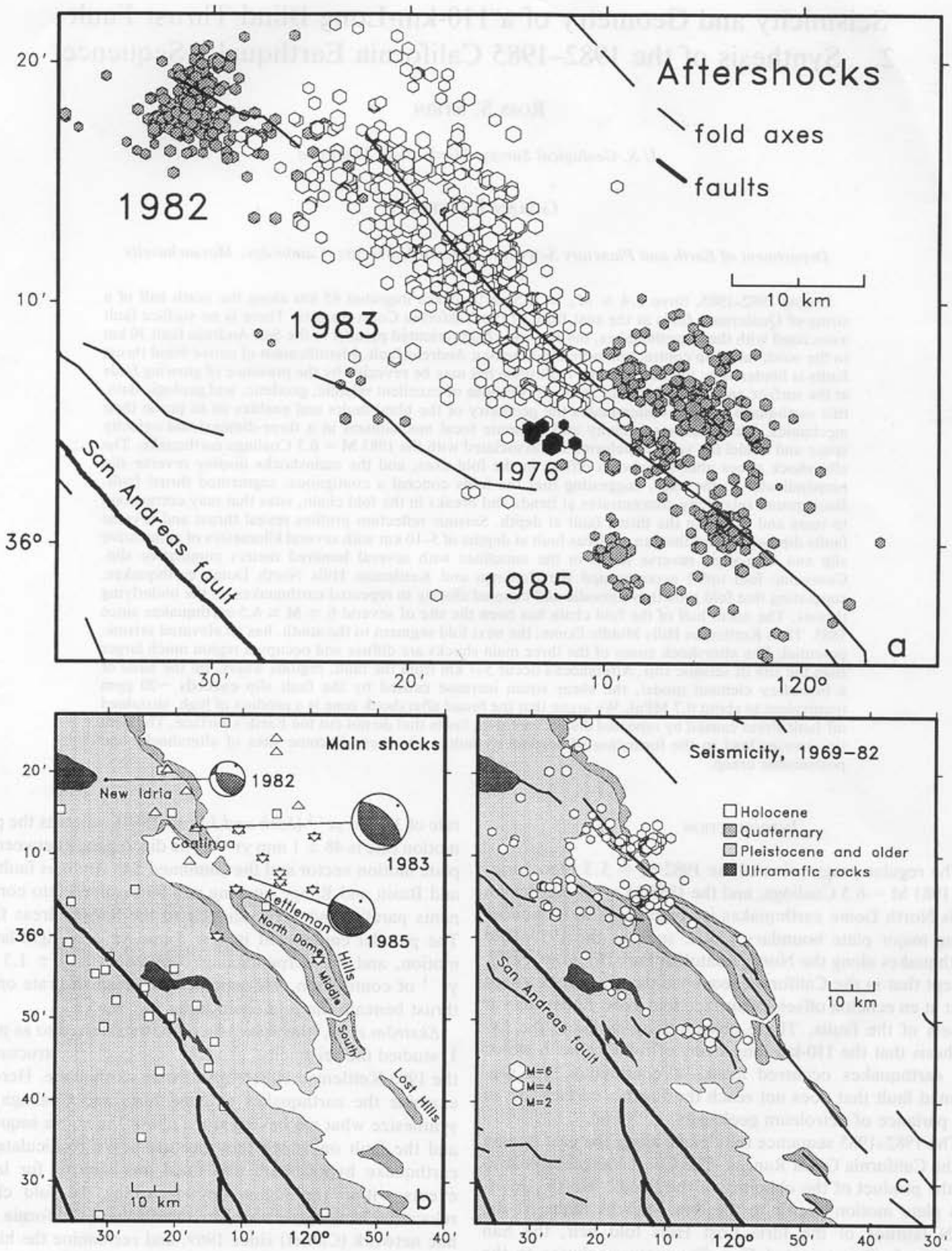

Fig. 1. (*a*) Relocated aftershock sequences of the 1982 New Idria (shaded hexagons, northwest), 1983 Coalinga (open hexagons), 1985 Kettleman Hills (shaded hexagons, southeast), and the 1976 Polvadero (solid hexagons) earthquakes. Fold axes largely from *Zigler et al.* [1986] and *Namson and Davis* [1988]. (*b*) Map showing permanent (squares) and 1983 (triangles) and 1985 (stars) Calnet stations used to locate the earthquakes. Equal-area, lower hemisphere projections of focal spheres for the 1982, 1983, and 1985 shocks are shown with compressional quadrants shaded. (*c*) Relocated seismicity 10–60 km northeast of the San Andreas fault during 1969 to September 1982 (location error ≤ 1.5 km).

TABLE 1. Mainshock Source Parameters

Parameter	1976 Polvadero	1982 New Idria*	1983 Coalinga†	1985 Kettleman Hills‡
Date	Jan. 14, 1976	Oct. 25, 1982	May 2, 1983	Aug. 4, 1985
Time, UT	2143	2226	2342	1201
Latitude/Longitude	36.072°N, 120.211°W	36.317°N, 120.507°W	36.221°N, 120.292°W	36.118°N, 120.150°W
Strike	110°	154°	145°	142°
Dip	25°SW	41°SW	30°SW	12°SW
Rake	80°	137°	100°	109°
Depth, km	10.1	14.0	9.7	10.1
Moment, dyn cm	1.5×10^{23}§	1.8×10^{24}	4.7×10^{25}	1.6×10^{25}

*From *Ekström and Dziewonski* [1985].
†From *Eberhart-Phillips* [1990] except for moment, which is from *Sipkin and Needham* [1990].
‡From paper 1.
§Conversion from M_L (4.7);

and geologic profiles across the fold to investigate how such structures develop.

Seismicity of the Fold Chain

Five $6 \geq \mathbf{M} \geq 6.5$ documented events have taken place along the north half of the 110-km-long fold chain. The best recorded 1982–1985 sequence (Figure 1) is described briefly here, relocated using the three-dimensional velocity model of *Eberhart-Phillips* [1989, 1990].

New Idria Earthquake

The 1982 New Idria $M_W = 5.4$ earthquake occurred 6 months before the Coalinga shock. The mainshock struck beneath the New Idria anticline, and the aftershock zone abutted the subsequent Coalinga aftershock zone (see Figures 1*a* and 1*b*). *Scofield et al.* [1985] obtained a mainshock focal depth of 7.3 km, whereas we find a depth of 14 km, deeper than both the Coalinga and Kettleman Hills events (mainshock parameters, Table 1). The centroid moment tensor focal mechanism of the New Idria earthquake [*Ekström and Dziewonski*, 1985] is consistent with reverse motion on a shallowly dipping fault, such as the ramp thrust, or on a steeply dipping plane extending into the core of the anticline (Figure 2*a*). Aftershocks cluster at 6- to 16-km depth but do not delineate a single plane. The aftershocks also locate near the fold axis of *Namson and Davis* [1988] (Figure 3*a*).

Coalinga Earthquake

The 1983 $M_W = 6.5$ Coalinga mainshock struck beneath the Coalinga fold axis at a depth of 10 km [*Eaton*, 1990], equidistant from the echelon fold offsets to the north and south (Figures 1*a* and 1*b* and Table 1). The aftershocks [from *Eberhart-Phillips*, 1989] extend between the fold offsets but are widely dispersed in cross section, with a depth range of 3–13 km (Figure 2*b*). The events are projected onto the cross section of *Wentworth and Zoback* [1989] under the assumption that the fold structure is continuous along the strike of the Coalinga fold axis.

Kettleman Hills Earthquake

The Kettleman Hills North Dome main shock resulted from slip on a thrust fault dipping gently southwest at about 10-km depth (paper 1). The mainshock, several foreshocks, and the northernmost aftershocks occurred at a 2-km right step in the fold axis, which coincides with the south limit of the Coalinga aftershocks. In cross section, the Coalinga and Kettleman Hills aftershocks look similar, except that at Kettleman Hills, the aftershocks lie about 6 km farther updip (northeast) of the fold axis (compare Figures 2*b* and 2*c*). The rupture duration of the Kettleman Hills earthquake was about 4 times longer than is common for an event of this size ($M_W = 6.1$; see Table 1), resulting in a long-period and geodetic moment much larger than that deduced from local seismograms.

Polvadero Sequence

The January 1976 earthquakes occurred 10 km southwest of the 1985 Kettleman Hills main shock near the Polvadero Gap, the topographic and structural saddle between the Coalinga and Kettleman Hills anticlines, and the boundary of the subsequent Coalinga and Kettleman aftershock zones (Figure 1*a*, solid hexagons). *Eaton et al.* [1983] suggested that the Polvadero (formerly "Avenal") and 1982 New Idria events outlined a seismic gap filled by the 1983 Coalinga earthquake. We examined the Polvadero sequence to study segmentation of the fold chain, reanalyzing the original Calnet seismograms and recalculating first motion focal mechanisms for the six largest shocks.

The $M_L = 4.7$ mainshock has the best constrained solution, with one plane dipping steeply southwest, in the opposite direction to the Kettleman Hills mainshock (Figure 3*b* and Table 1). Although the focal mechanisms for the six largest Polvadero earthquakes are poorly constrained, nearly all solutions show reverse faulting with varying amounts of strike-slip motion (Figure 3*b*). The *P* axes of allowable solutions orient east-northeast. The quality of the nine best constrained 1976 earthquake locations is equal to that of the 1985 events, with the mainshock at 10 km depth. Thus the 1976 sequence occurred on a high-angle reverse fault at the same depth as the 1985 Kettleman Hills shock but 10 km west of the tip of the thrust fault.

Historical Earthquakes

Several large earthquakes have occurred along the north half of the fold chain, including two $M \sim 6.5$ events (1885 and 1983 Coalinga), three $M \sim 6$ events (1905 [*Toppozada et al.*, 1990], July 22, 1983, Nuñez shock [*Rymer et al.*, 1990], and the 1985 Kettleman Hills event), and at least two $M \sim 5.5$ shocks (1926 Idria and 1982 New Idria). Using seismograms recorded at Berkeley, the Lick Observatory, and Pasadena, *Byerly* [1927] located the 1926 Idria shock at lat

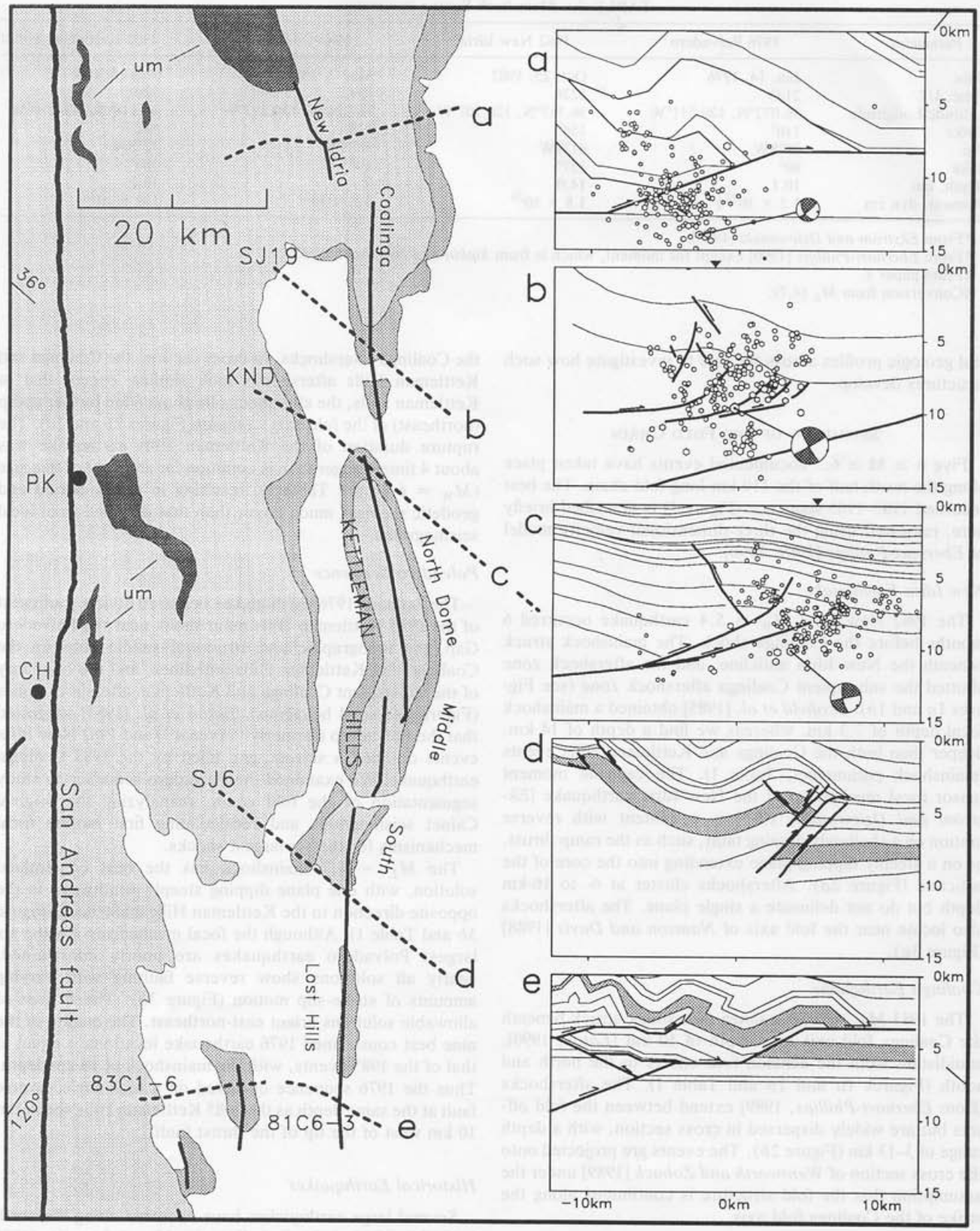

Fig. 2. Structural and seismic cross sections projected normal to the fold chain at (*a*) New Idria, (*b*) Coalinga, (*c*) Kettleman Hills North Dome, (*d*) Kettleman Hills South Dome, and (*e*) the Lost Hills. A subset of aftershocks projected on profiles in Figures 2*a*–2*c* with back-hemisphere projections of the main shocks shown. Arrowheads on the surface of Figures 2*b* and 2*c* show the position of peak coseismic uplift. Figure 2*a* is a balanced section constructed largely from oil well logs by *Namson and Davis* [1988]; the others (Figure 2*b*, *Wentworth and Zoback* [1989]; Figure 2*c*, *Meltzer* [1989]; and Figure 2*d*, R. Bloch et al. (submitted manuscript, 1992) and Figure 2*e*, *Medwedeff* [1989]) rely on seismic reflection and refraction data, supplemented by oil well logs. PK, Parkfield; CH, Cholame.

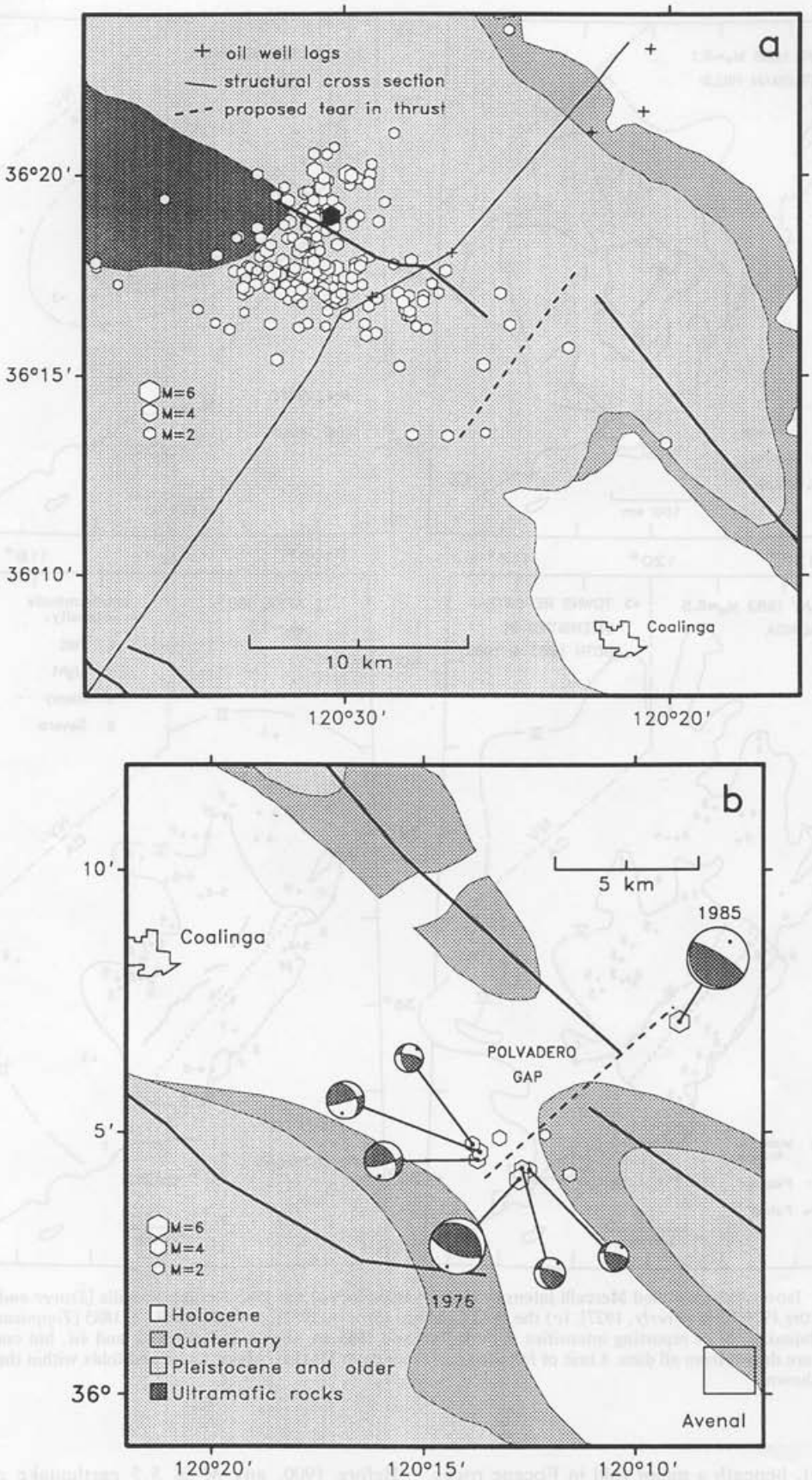

Fig. 3. (*a*) Map of the New Idria sequence (solid hexagon, main shock) and geologic traverse by *Namson and Davis* [1988]. (*b*) Map of 1976 Polvadero events with location errors ≤1.5 km, showing first-motion focal mechanisms for main shock ("1976") and five largest shocks. Location and focal mechanism for the 1985 Kettleman Hills earthquake are shown for reference.

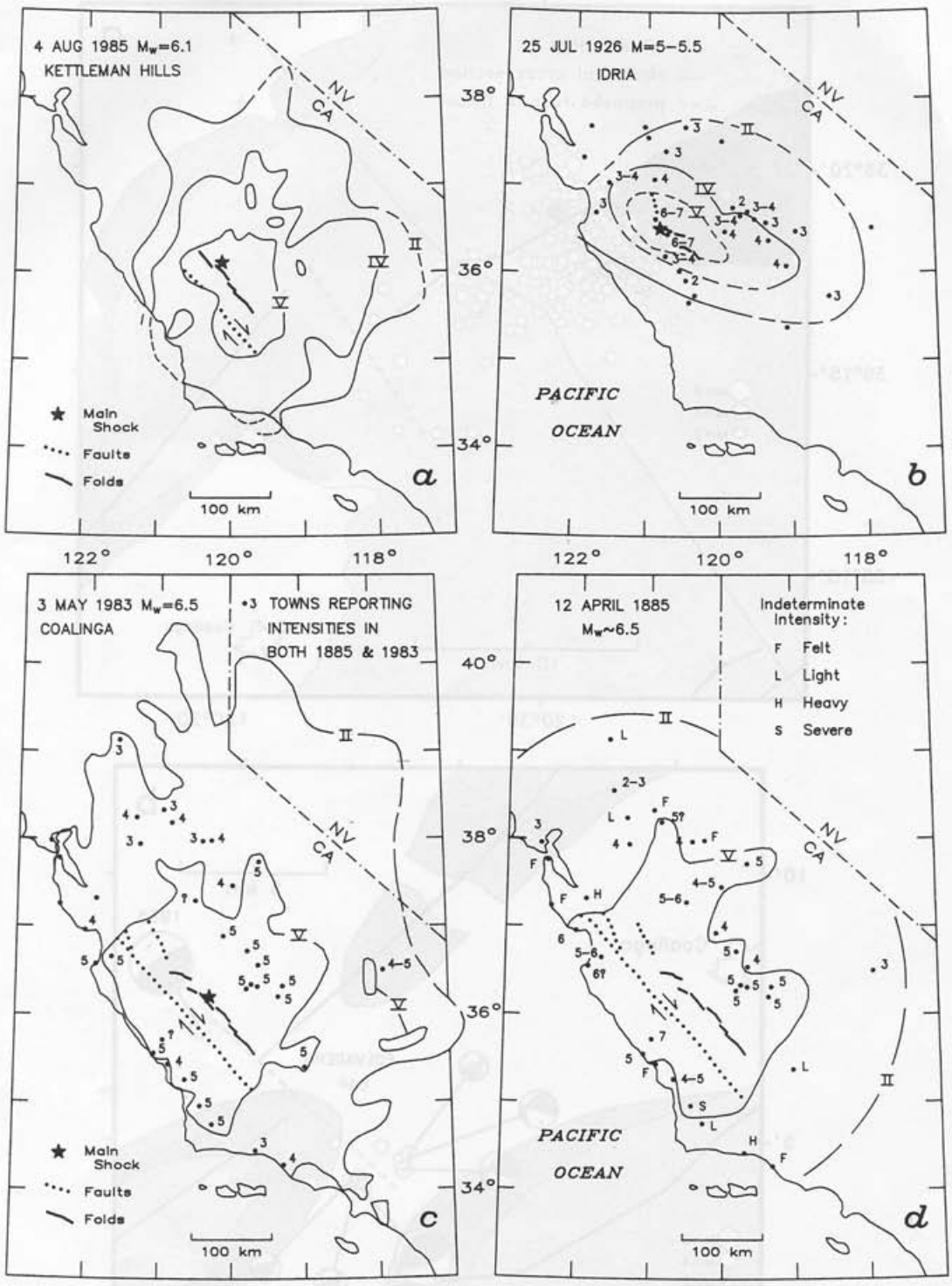

Fig. 4. Isoseismal (modified Mercalli intensity (MMI)) maps for (*a*) the 1985 Kettleman Hills [*Stover and Brewer*, 1991], (*b*) the 1926 Idria [*Byerly*, 1927], (*c*) the 1983 Coalinga [*Stover*, 1983], and (*d*) April 12, 1885 [*Toppozada et al.*, 1981] earthquakes. Sites reporting intensities in both 1983 and 1885 are shown in Figures 4*c* and 4*d*, but contours in Figure 4*c* are drawn from all data. Limit of felt area corresponds to MMI II. Major faults and folds within the MMI V zone are shown.

36.5°N (Figure 4*b*), beneath a major fold in Eocene rocks. *Toppozada et al.* [1990] used the felt area to estimate magnitude of 5.5 for the 1926 Idria shock. The 1926 Coalinga earthquake was located by isoseismals by *Townley and Allen* [1939] and assigned $M = 5$ by *Toppozada et al.* [1978]. Before 1900, any $M \leq 5.5$ earthquake could have gone undetected in this region due to the sparse population.

The April 12, 1885, earthquake, the largest shock to strike California between 1872 and 1892 [*Townley and Allen*, 1939], probably took place near the fold chain north of Coalinga.

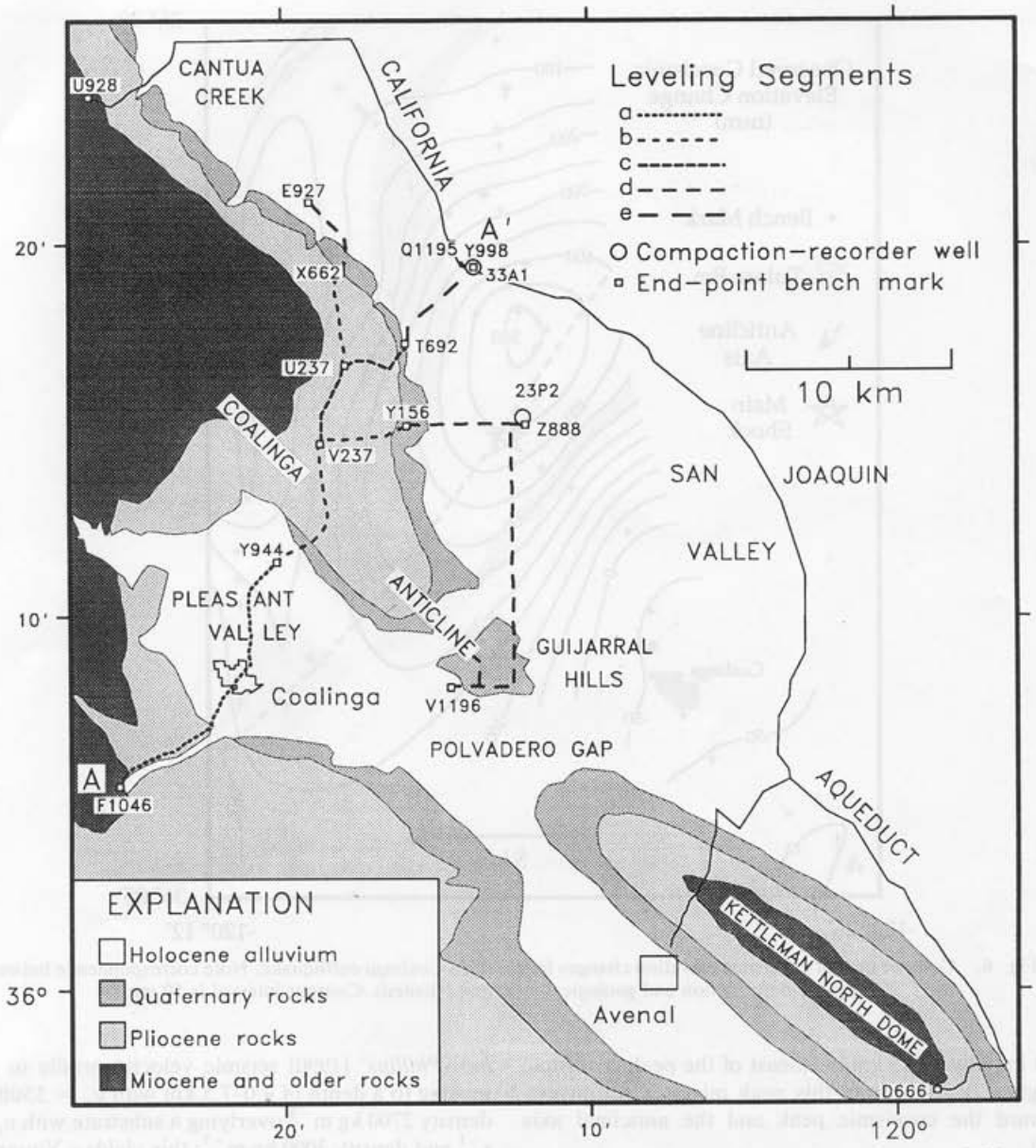

Fig. 5. Coalinga and Kettleman Hills leveling network, identifying Coalinga leveling segments subject to subsidence corrections listed in Table A3.

Toppozada et al. [1981] assigned the 1885 event $M = 6.2$ and placed it on the San Andreas fault 50 km north of Parkfield. However, the modified Mercalli intensity II and V isoseismal zones for 1885 and the 1983 Coalinga earthquakes are quite similar, with the 1885 isoseismals shifted 10–40 km northward (Figures 4*c* and 4*d*). This similarity suggests that both events have $M = 6.5$ and that the 1885 event struck east of the San Andreas on or near the fold chain. No large deformation event is seen in the late Holocene record of Los Gatos Creek at Coalinga during the past 250 years [*Atwater et al.*, 1990], suggesting that the 1885 shock probably did not take place along the Coalinga segment. The 1885 isoseismals might place the 1885 event near New Idria, but the Kettleman Hills event showed that the rupture propagation direction changes the intensity pattern from being symmetric about the slip zone (Figure 4*a*), leaving as much as a 50-km uncertainty in the 1885 earthquake source.

Coalinga Earthquake Deformation

Observations of the deformation that accompanied the Coalinga earthquake suggest that repeated earthquakes built the Coalinga fold. Here we use the record of deformation to investigate the fault geometry and slip. By "coseismic deformation" we refer to the elevation change between surveys in February 1969 to March 1982 and those in June 1983 to September 1984, which could contain some non-earthquake deformation (leveling network, Figure 5; uplift contours, Figure 6; corrections for leveling errors and non-tectonic subsidence, see the appendix). The axis of coseismic uplift and the fold axis coincide (Figure 7), and the areal distribution of uplift mimics the geologic expression of the fold (Figure 6). Deformation during the first 4 years after the Coalinga earthquake amounts to 20–22% of the coseismic deformation, or about 110 mm (Figure 8). The peak postseis-

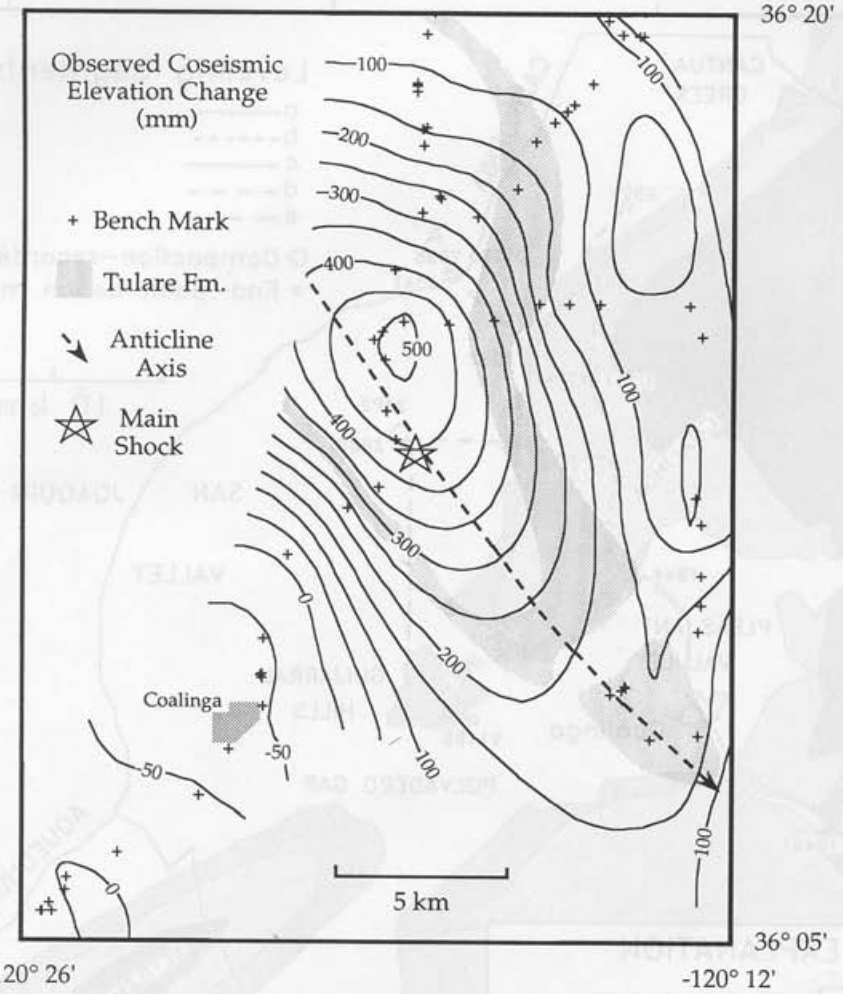

Fig. 6. Contour map of coseismic elevation changes for the 1983 Coalinga earthquake. Note correspondence between earthquake deformation and geological structure (shaded). Contour interval is 50 mm.

mic uplift initially lies 5 km northeast of the peak coseismic uplift (Figure 7); over time, this peak migrates southwestward toward the coseismic peak and the anticlinal axis (Figure 9).

We seek to use the observed deformation to identify the fault surface from the two nodal planes of the mainshock and to learn the fault shape and slip magnitude. The geodetic observations are modeled by a dislocation surface (formed by an array of point sources at 1 × 1 km spacing) embedded in an elastic Earth. We consider only uniform reverse dip slip, in keeping with the focal mechanism for the mainshock, and because the elevation changes are insensitive to small variations in rake. Because bench marks are well distributed and the signal/noise ratio of the data is high (6.1), we do not restrict the fault surface to being rectangular or planar. Following the procedure outlined in paper 1 to minimize the weighted residuals, we test a range of geometries in 60,000 trials. The fault length, depth, position, strike, dip, curvature, and width at each end are systematically varied; the mean fault slip and zero-elevation change datum are solved by least squares.

We applied a depth correction to the elastic half-space results to account for the presence of compliant sedimentary rocks of the Great Valley sequence overlying stiffer Franciscan Complex and basement rocks. We simplified *Eberhart-Phillips*' [1990] seismic velocity profile to a layer extending to a depth of 4.0–7.5 km with v_p = 3500 m s^{-1} and density 2700 kg m^{-3} overlying a substrate with v_p = 6250 m s^{-1} and density 3000 kg m^{-3}; this yields a Young's modulus contrast of 3.5. The boundary between the upper and lower regions coincides with the base of the shaded strata in Figure 10, and with the 5000 m s^{-1} contour of *Eberhart-Phillips*' [1990] Figure 4*b*. Using a two-dimensional boundary element model [*King and Ellis*, 1991], we found that the half-space solution underestimates the depth of the fault by 1.0 km for the reverse fault and 1.5 km for the thrust fault, because the low-modulus surface layer concentrates the surface deformation. The fault dip, slip, fault area, and moment do not change. These results are in qualitative agreement with findings of *Rodgers and Rizer* [1981] and *Reches and Zoback* [1990].

Coseismic slip. Gently southwest dipping thrust faults (Figures 10*a* and 10*b*) and steeply northeast dipping reverse faults (Figures 10*c* and 10*d*) satisfy the geodetic observations equally well. The misfit/noise (M/N) ratio for the best model in each case is 1.66, indicating that most signal has been modeled to within its noise level. (M/N = 1 means that the model residuals are equal to the expected noise in the data; we define M/N in the appendix of paper 1). Although a range of source parameters can fit the observations, the

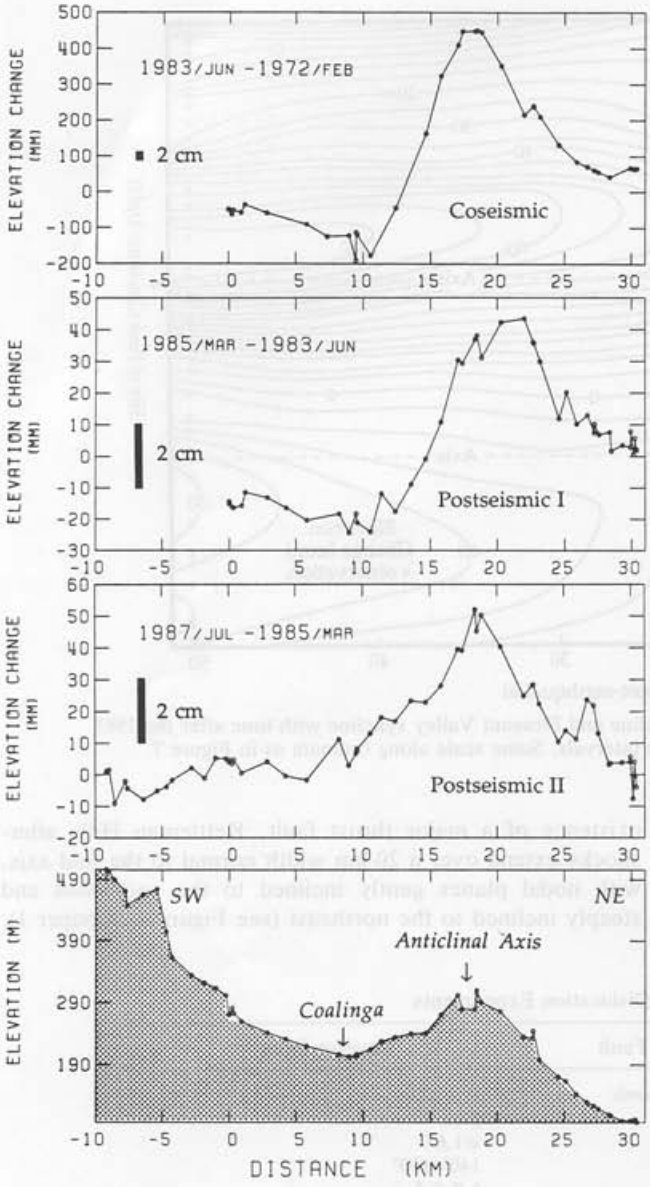

Fig. 7. Corrected deformation profiles projected along azimuth N50°E across the Coalinga anticline (route A–A′) for three epochs, with route topography.

acceptable range for which M/N < 1.7 is compatible with the focal mechanism of the mainshock (fault strike, 140°–150°, and dip, 10°–20° SW or 65°–75° NE). The geodetic moment is 6–10 × 10^{25} dyn cm, equivalent to **M** = 6.5 ± 0.1. *Choy* [1990] found a moment of 2.7 × 10^{25} dyn cm from broadband body waves; *Sipkin and Needham* [1990] obtained 4.7 × 10^{25} dyn cm using teleseismic data, marginally smaller than the geodetic estimate.

Among acceptable fault geometries, thrust faults pass within 1.5 km of the mainshock hypocenter (Figures 10*a* and 10*b*), whereas reverse faults tend to locate several kilometers southwest of the mainshock (Figures 10*c* and 10*d*). Thrust faults lying several kilometers above the main shock also fit the observations. In map view, the width (downdip fault dimension) of models for which M/N ≤ 1.7 diminishes southeastward toward the Guijarral Hills. This geometry mimics the geologic structure and aftershock zone, which becomes narrower to the southeast (Figures 1*a* and 1*b*). Strongly listric faults, which are concave upward in profile, degrade the fit. Figure 11 shows the detailed fit for the fault of Figure 10*a*.

Postseismic slip. The postseismic observations furnish fewer constraints than the coseismic data because only the main leveling line (A–A′, Figures 5 and 11) was surveyed repeatedly after the earthquake. The condition that the slip surface intersects the main shock is also no longer requisite for postseismic models. Because we extended the leveling line southwestward in 1985, the first ("Post I," 1983.5–1985.2) and second ("Post II," 1985.2–1987.6) periods were tested separately. Both reverse and thrust faults can fit the data appreciably better than the expected noise, M/N ≥ 0.78 (Table 2). The slip surface corresponding to the Post I period extends several kilometers northeast of the coseismic slip, because the peak uplift lies 3–4 km northeast of the coseismic uplift (Figure 7). Post I slip extending updip of a coseismic thrust fault (Figures 10*a* and 10*b*, dotted lines), or downdip of a coseismic reverse fault (Figures 10*c* and 10*d*) satisfy the observations. Both sites are located within aftershock clusters, but because the aftershocks took place before the measured postseismic slip, the association need not be causal. The Post II deformation corresponds closely to the site of coseismic slippage.

DISCUSSION

Dominance of the Thrust Fault

Although slip on either a northeast dipping reverse or a southwest dipping thrust fault can explain the seismicity and geodesy of the Coalinga and Kettleman Hills earthquakes, we infer from these data that slip occurred principally on a southwest dipping thrust fault, at 8–14 km depths. At Kettleman Hills North Dome the axis of coseismic uplift locates 4 km northeastward of the anticlinal axis (see Figure 8 in paper 1). As we argue in paper 1, this suggests that the fold and underlying thrust are propagating northeastward. The postseismic deformation at Coalinga is also most simply explained by slip propagating to the northeast, beyond the coseismic fault tip, as in Figures 10*a* and 10*b*. These observations also could be explained by successive genera-

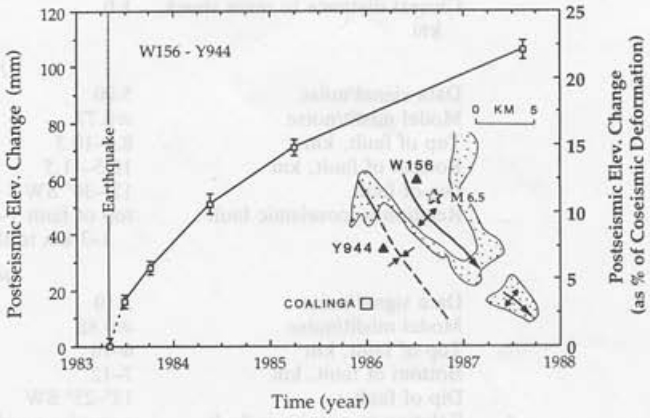

Fig. 8. Time history of growth of the Coalinga anticline with respect to the Pleasant Valley syncline (inset) following the 1983 Coalinga earthquake. First (dashed) interval extrapolated from subsequent observations by using a third-degree polynomial.

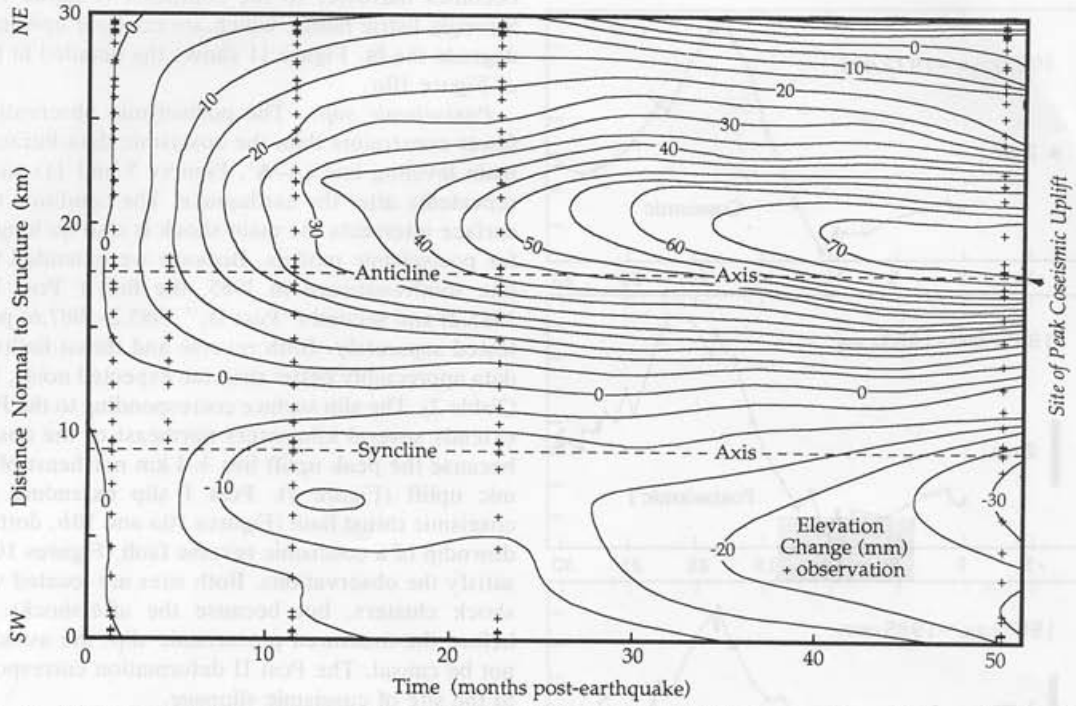

Fig. 9. Migration of deformation across the Coalinga anticline and Pleasant Valley syncline with time after the 1983 earthquake; observations (crosses) contoured at 5-mm intervals. Same scale along ordinate as in Figure 7.

tions of NE dipping reverse faults, each forming farther to the northeast, but none of the seismic reflection profiles shows midcrustal reverse faults northeast of the fold.

Earthquake focal mechanisms also lend support to the existence of a major thrust fault. Kettleman Hills aftershocks extend over a 20-km width normal to the fold axis, with nodal planes gently inclined to the southwest and steeply inclined to the northeast (see Figure 3 of paper 1).

TABLE 2. Summary of Dislocation Experiments

Parameter	Thrust Fault	Reverse Fault
	Coseismic	
Data signal/noise	6.09	6.09
Model misfit/noise	≥1.66	≥1.67
Fault strike	140°–150°	140°–150°
Top of fault, km	7.0–8.0	6.0–8.5
Bottom of fault, km	8.5–9.5	9.5–13.5
Dip of fault	15°–20° SW; 30° at top of fault	70°–75° NE
Fault slip, m	1.5–3.0	2.3–8.4
Geodetic moment M_0, dyn cm	$6–10 \times 10^{25}$	$5–9 \times 10^{25}$
Closest distance to main shock, km	1.0	2.0
	Post I	
Data signal/noise	5.00	5.00
Model misfit/noise	≥0.77	≥0.78
Top of fault, km	8.0–10.5	7.5–10.5
Bottom of fault, km	10.5–11.5	10.0–14.5
Dip of fault	15°–30° SW	60°–75°NE
Relation to coseismic fault	top of fault 1–3 km deeper and 1–3 km to the NE	top of fault 1–4 km deeper and 1–2 km to the NE
	Post II	
Data signal/noise	2.10	2.10
Model misfit/noise	≥0.62	≥0.60
Top of fault, km	6–10	6–9
Bottom of fault, km	7–12	7–14
Dip of fault	13°–25° SW	63°–73° NE
Relation to coseismic fault	occupies nearly the same position as coseismic fault	can coincide with Post I or near the coseimic fault

Post I period is 1983.5–1985.2; Post II period is 1985.2–1987.6.

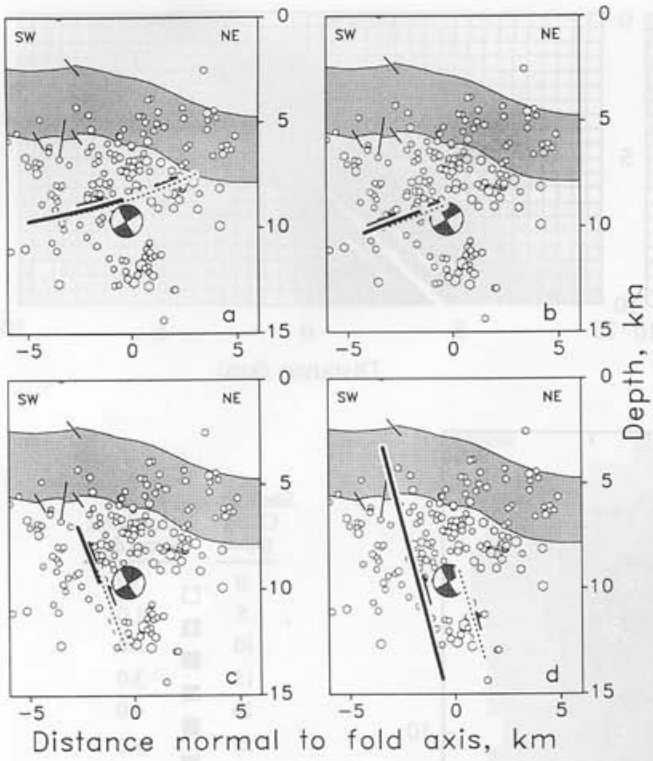

Fig. 10. Cross sections of representative dislocation models that satisfy the geodetic data, projected along azimuth N55°E, with a back-hemisphere projection of the Coalinga main shock. Folded strata and small fault offsets are from seismic reflection profile SJ19. Coseismic models (bold lines) have M/N ≤ 1.7, and postseismic (dotted lines) models have M/N ≤ 0.8. (*a*) and (*b*) SW dipping thrust faults, (*c*) and (*d*) NE dipping reverse faults.

Most aftershocks lie within a few kilometers of *Meltzer*'s [1989] proposed thrust fault, suggesting that minor slip along the thrust produced aftershocks well to the southwest of the main rupture. In addition, the 1976 Polvadero earthquake lies 6 km southwest of the Coalinga fold axis (Figure 3*b*). The proximity of the 1976 event to the Coalinga-Kettleman fold offset suggests that the thrust faults extend southwestward and are offset or torn at the step in the fold axes. Weak alignment of the southernmost 1982 New Idria aftershocks extending southwestward from the Idria-Coalinga fold offset (Figure 3*a*) also suggests a tear in the thrust at depth.

Seismic reflection profiles also furnish evidence that a southwest dipping thrust fault underlies the Idria–Coalinga–Kettleman Hills–Lost Hills fold chain. The profiles display faint, discontinuous reflections dipping southwest at 8–10 km depth beneath the Coalinga and Kettleman Hills North Dome anticlines (Figures 2*b* and 2*c*), and strong reflections beneath Kettleman Hills South Dome (Figure 2*d*). Reverse faults dip 45° both to the northeast and southwest, but the northeast dipping faults have minimal (<200 m) throw. In contrast, the main southwest dipping fault displays a cumulative throw of 3.5 km and extends to a depth of at least 9 km at Kettleman South Dome. *Yeats et al.* [1988] also found high-angle faults with negligible cumulative slip in the core of the Ventura Avenue anticline, among the world's best studied active folds.

Fault propagation folding (in which a blind thrust propagates upward through the crust [*Meltzer*, 1989; *Wentworth and Zoback*, 1989; R. Bloch et al., Style and magnitude of tectonic shortening normal to the San Andreas fault across Pyramid Hills and Kettleman Hills South Dome, California, submitted to *Geological Society of America Bulletin*, 1992) and fault-bend folding (in which a horizontal decollement ramps upward to a higher decollement level [*Suppe*, 1983; *Namson and Davis*, 1988; *Medwedeff*, 1989]) have been proposed for parts of the Idria–Coalinga–Kettleman Hills–Lost Hills fold chain. Both structures are compatible with slip on a low-angle thrust fault and with eastward propagation and growth of the overlying anticlines. But the seismic and geodetic data furnish no evidence for an active horizontal slip surface northeast of the earthquake hypocenters locations where, in fault-bend folding, a horizontal decollement would lie. Instead, high-angle mechanisms northeast of the main shock hypocenters (see paper 1, Figures 3*a* and 3*b*) and the concentration of aftershocks extending northeastward and upward of the main shock hypocenters of both the Coalinga and Kettleman earthquakes are more consistent with fault propagation folding.

The Coalinga–Kettleman Hills–Lost Hills chain closely parallels the San Andreas fault, which lies 30 km to the southwest. *Simpson et al.* [1988] found evidence for coupling of the Coalinga and Kettleman Hills events with creep and earthquakes on the San Andreas fault at Parkfield, and *Namson and Davis* [1988] and *Eaton and Rymer* [1990] suggest that the thrust cuts the San Andreas fault and continues westward. The amount of contraction normal to the San Andreas taken up by the thrust fault can be gaged from its Quaternary fault slip rate. The Coalinga fold has a structural relief of about 1000 m, and Kettleman Hills North Dome has 900 m, most of which accumulated during the past 2–3 m.y. [*Stein and King*, 1984], yielding a fold uplift rate of about 0.4 mm yr^{-1}. Since 1.5–3.0 m of fault slip yielded 0.7 m of coseismic fold growth at Coalinga, a fault slip rate of

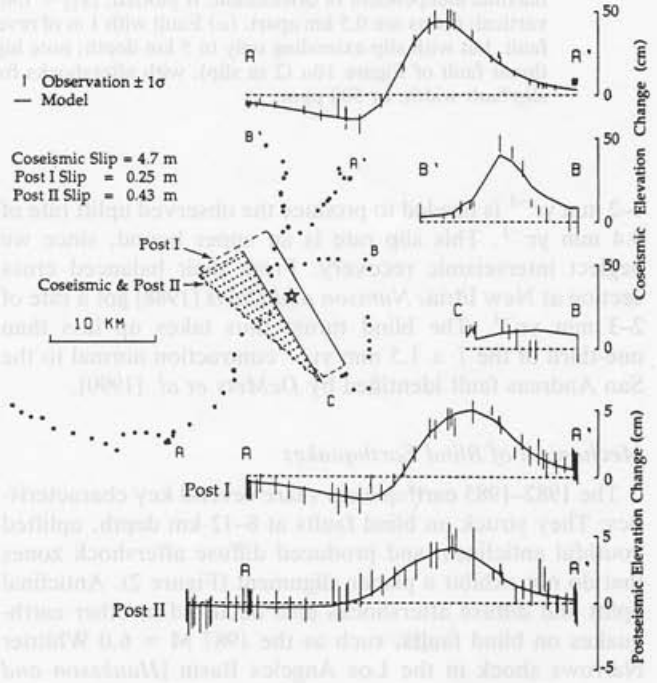

Fig. 11. Fit of representative coseismic and postseismic model to geodetic observations for the 1983 Coalinga earthquake. Cross section of model is shown in Figure 10*b*. Profiles A–A′ and C–B are projected along N55°E; B′–B is projected along N35°W.

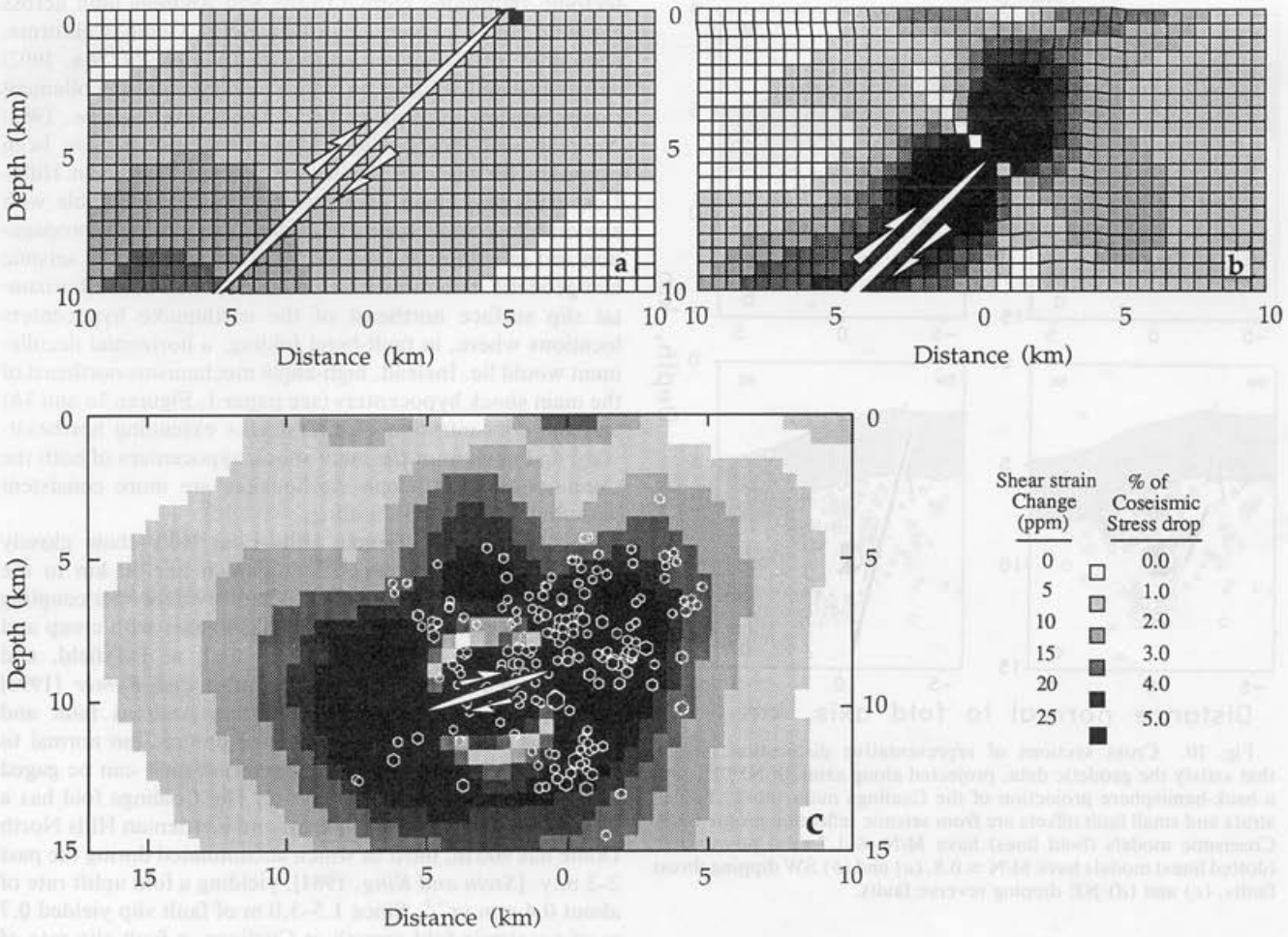

Fig. 12. Boundary element visualizations of the strain change produced by blind and surface-cutting faults embedded in an elastic half-space; faults are infinite in length along strike. Deviatoric shear strain, or the shear strain maxima independent of orientation, is plotted, $[\varepsilon_{12}^2 + 1/4(\varepsilon_{11} - \varepsilon_{22})^2]^{1/2}$, where the unit vector 1 is horizontal and 2 is vertical; nodes are 0.5 km apart. (*a*) Fault with 1 m of reverse slip extending from a depth of 15 to the surface. (*b*) Same fault, but with slip extending only to 5 km depth; note high shear strain associated with blind fault. (*c*) Coalinga blind thrust fault of Figure 10*a* (2 m slip), with aftershocks from Figure 10 superimposed. Earthquake strain drop is fault slip/fault width, or 500 ppm.

1–2 mm yr^{-1} is needed to produce the observed uplift rate of 0.4 mm yr^{-1}. This slip rate is an upper bound, since we neglect interseismic recovery. From their balanced cross section at New Idria, *Namson and Davis* [1988] got a rate of 2–3 mm yr^{-1}. The blind thrust thus takes up less than one-third of the 7 ± 1.5 mm yr^{-1} contraction normal to the San Andreas fault identified by *DeMets et al.* [1990].

Mechanism of Blind Earthquakes

The 1982–1985 earthquakes share several key characteristics: They struck on blind faults at 8–12 km depth, uplifted youthful anticlines, and produced diffuse aftershock zones that do not exhibit a planar alignment (Figure 2). Anticlinal uplift and diffuse aftershocks also occurred in other earthquakes on blind faults, such as the 1987 **M** = 6.0 Whittier Narrows shock in the Los Angeles Basin [*Hauksson and Jones*, 1989; *Lin and Stein*, 1989], the 1985 **M** = 6.6 and 6.8 Nahanni, Canada, earthquakes [*Wetmiller et al.*, 1988], and the 1964 **M** = 7.6 Niigata, Japan, earthquake [*Mogi et al.*, 1964; *Satake and Abe*, 1983].

We argue that the diffuse aftershocks and distributed secondary faults result from high remanent stresses produced by earthquakes on blind faults in the seismogenic part of the crust. Stresses at depths below about 10 km relax slowly during the interseismic period by ductile flow and creep. Reverse faults that cut the Earth's surface (Figure 12*a*) also relieve most shear stress in the upper crust, because the fault cuts the free surface, which cannot store in-plane shear. Thus, over many earthquake cycles, the crust acts as a plate cut by a throughgoing fault, with nearly complete relaxation of stress. In contrast, because the tip of a blind fault is embedded in the crust, the stress concentration near the fault tip will be relaxed neither by proximity to a free surface nor by ductile flow below (Figure 12*b*), as shown by *Rodgers and Rizer* [1981].

A cross section of the shear strain change caused by coseismic slip at Coalinga (Figure 12*c*) was generated by using the boundary element model of *King and Ellis* [1990]. Aftershocks of the Coalinga earthquake lie within the region that sustained a predicted shear strain increase of >20 ppm

(equivalent to >4% of the coseismic stress drop, or about 0.7 MPa). Aftershocks are absent in regions with strain change ≤ 5 ppm. A lobe of increased shear strain occurs above the fault at depths of 2–7 km, site of high-angle reverse faults and aftershocks at Coalinga and Kettleman Hills (compare Figure 12*c* to Figure 10*a*). This suggests that these shallow secondary faults need not root into the thrust below but may instead be the product of concentrated strains produced by slip at depth. An exception to the correlation between strain increases and aftershocks is seen near the downdip edge of the fault, perhaps because interseismic creep downdip from the fault relieves stresses. Note that while the slip associated with the aftershocks will modify the predicted strain pattern, the seismic moment of the mainshock is an order of magnitude greater than that of the summed moment of the aftershocks, so that the changes in strain will be minor.

The region with a >20 ppm shear strain increase containing the aftershocks coincides with the site of possible postseismic slippage shown in Figure 10*a* and is 3 times wider than the site of fault slip. The region surrounding the fault must thus have been within ~0.5 MPa of failure before the earthquake for the off-fault stress increase to have triggered aftershocks. Therefore there can be little interseismic relaxation of stress at the 5–10 km depth of the aftershocks. High fluid pressures may also promote secondary fault failure and aftershocks by reducing the frictional strength of the rock. *Yerkes et al.* [1990] identified the Kettleman and Lost Hills as sites of abnormally high fluid pressures measured at depths to 7 km, and *Eberhart-Phillips* [1990] detected low-velocity zones beneath the Coalinga anticline at depths of 4–6 km, which she attributed to high fluid pressure.

Earthquake Migration Along the Fold Chain

The 1982–1985 earthquake sequence started at the north end of the fold chain and migrated 65 km to the midpoint along the chain. In contrast, no $M > 6$ earthquake has struck on or south of Kettleman Hills Middle Dome during the twentieth century. Because the age and rate of uplift are similar throughout the chain, we suggest that there is an elevated seismic risk at Kettleman Hills Middle and South Domes, although we lack sufficient data to quantify that potential. *Wesson and Nicholson* [1988] advanced a similar hypothesis, although they lacked data to confirm that the entire Kettleman North Dome segment had ruptured in 1985, as we show in paper 1. The main thrust fault appears to ramp up from perhaps 15 km depth at the north end of the chain to 5 km at the south end (Figure 2), but as this falls within seismogenic depths, we see no reason why earthquakes would not take place south of the 1985 rupture zone. South of Middle Dome, the Kettleman Hills South Dome–Lost Hills anticline is the longest structurally continuous segment of the chain, 38 km, and thus may be capable of a M = 6.5–7.0 earthquake.

Whether a Kettleman Hills Middle Dome earthquake will continue the sequence is not clear. First, background seismicity during the past 20 years (Figure 1*c*) and large earthquakes since 1885 have been more abundant north of Middle Dome. Second, from the fragmentary historical record, the previous cycle of earthquakes did not migrate, and so the ordered progression of the recent sequence might not continue. Finally, the north half of the chain is next to the creeping section of the San Andreas fault (creep extends to Cholame, Figure 2). Shear strain is not accumulating north of Parkfield, whereas south of Cholame the fault has been locked since the great 1857 earthquake. Thus thrust earthquakes along the fold may be coupled to the cycle of great strike-slip events on the San Andreas fault.

CONCLUSION

We have presented seismic, geodetic, and geologic evidence here and in paper 1 that the leading edge of a continuous segmented thrust fault dipping gently toward the San Andreas underlies the 110-km-long Idria–Lost Hills fold chain. We have argued that the 1982, 1983, and 1985 earthquakes took place on this fault. At its north end, the fault lies at a depth of 15 km; through a series of tears and ramps, it reaches a depth of perhaps 5 km at its south end. High-angle reverse faults, dipping both toward and away from the San Andreas fault, are abundant in the cores of the anticlines that overlie the fault tip and at offsets of the fold axes, and some seismicity occurs on these reverse faults. We have further argued that the Kettleman Hills Middle Dome has an elevated seismic potential for an $\mathbf{M} \leq 6.5$ earthquake, and the southernmost Kettleman Hills South Dome–Lost Hills segment could produce an $\mathbf{M} \leq 7$ earthquake.

Diffuse aftershock zones, particularly when viewed in cross section, are a key feature of large earthquake rupture on blind faults. This makes it difficult to select the fault from the nodal planes, but it also affords insight into the process of blind fault rupture. Blind faults do not cut the Earth's surface, and thus stress near the fault tip remains high. The rock containing the fault therefore remains close to its failure threshold, and the stress increase off the fault will induce failure, realized by secondary fracture, aftershocks, or creep. Slow slip at Kettleman Hills and delayed slip at Coalinga may be products of high off-fault stresses, distributed secondary fractures, and elevated pore fluid pressures in the folds.

What are the implications of this earthquake sequence for other active folds? Perhaps most important is the realization that a thrust fault with a slip rate of just 2 mm yr^{-1} could be 100 km long and produce two M = 6.5 earthquakes in a century. The corresponding average uplift rate of the fold, 0.4 mm yr^{-1}, is close to the noise level of geodetic measurements and thus could escape detection during the interseismic period. A similar blind thrust fault in the Los Angeles Basin, for example, was not recognized until the 1987 $\mathbf{M}$ = 6.0 Whittier Narrows earthquake [*Davis et al.*, 1989; *Hauksson and Jones*, 1989; *Lin and Stein*, 1989]. The Idria–Lost Hills fold chain is readily identified only because it lies against undeformed strata. A fold within previously deformed or crystalline rocks would be all but invisible except during large earthquakes. Thus the number of active folds omitted from our global inventory of potential earthquake sites is unknown. Background seismicity is unlikely to reveal the presence of a simple thrust fault; instead, clusters of earthquakes at the bends and breaks in the fold chain are probably more diagnostic. We suggest that blind thrusts are best found by identifying active Quaternary folds from geodetic and geomorphic analysis and from seismic reflection and stratigraphic data.

TABLE A1. Coalinga Leveling Specifications

Survey Agency	Line Number	Survey Date	Order of Leveling (Double/Single Run)	Rerun Sections, %	Rejection Tolerance β, mm	Observed σ, mm	Assigned α, mm	Rod Calibration Facility†	Refraction Correction Method‡
NGS	L17723.1, 3, 15	Jan.–Feb. 1960	first (double)	12	4.0	1.38	1.3	NGS	solar radiation
NGS	L20605.1, 14, 25	March 1966	first (double)	7	4.0	1.26	1.3	NGS	solar radiation
NGS	L21703.21, 27, 29	Feb.–March 1969	second (double)	10	8.4	2.28	2.5	NGS	solar radiation
NGS	L22671.15, 16, 19–21	Feb.–March 1972	second (single)	10	8.4	2.00	2.5	NGS	solar radiation
CDWR	Rt-145, sheets 17–18	Feb.–March 1982	first (double)	12	3.0	1.54	2.5	USN	none
NGS	L24759	June 8–24, 1983	first (double)	6	4.0	0.91	1.3	NIST	observed gradient
NGS	L24779	Sept. 9–19, 1984	first (double)	7	4.0	1.44	1.3	NIST	observed gradient
NGS	L24878.1	March 2 to April 30, 1985	first (single)	8	3.0	1.15	1.3	NIST	observed gradient
NGS	L24904	March 4–22, 1985	first (single)	20	4.0	1.25	1.3	NIST	observed gradient
NGS	L25064	July 8 to Aug. 6, 1987	first (single)	36	4.0	1.32	1.3	NIST	observed gradient

$\sigma = 1/3\beta$ for normally distributed errors; assignments for α are more conservative than the observed σ.
*Only the CDWR survey used a leveling instrument (Zeiss Ni1 90843) susceptible to magnetic error, was field tested in 1989, and shows <0.6 mm km^{-1} error, too small to justify correction.
†NGS and U.S. Navy (USN), calibration by microscope; National Institute of Standards and Technology (NIST) calibration by laser interferometer.
‡Solar radiation model of *Holdahl* [1981]; observed gradient model uses mean temperature gradient measured per section. No correction was made to CDWR survey because field temperatures were not measured.

APPENDIX: LEVELING ACQUISITION AND REDUCTION

The primary source of leveling data is height measurements in a dense geodetic network surveyed by the National Geodetic Survey (NGS) four times before the 1983 earthquake and four times afterward (Figure 5 and Table A1). Parts were also surveyed by the California Department of Water Resources (CDWR) in 1982.

Leveling Errors

Random error is estimated from the agreement between forward and backward running of each section between bench marks (see the appendix of paper 1). A section is rejected if the forward and backward running do not agree within a prescribed tolerance β. If error is random, then σ propagates as $\alpha(S)^{1/2}$, where S is the distance (in kilometers) and α is in millimeters, and $\alpha \cong 1/3\beta$. This relation generally obtains when there are enough sections to form a reliable sample (Table 2). The typical rms random error for the coseismic period is about 10 mm. Systematic corrections for rod and refraction error are essential to measurement of the coseismic deformation because leveling practices and equipment changed during the period 1972–1983. All observations are corrected for level collimation, solid earth tides, thermal expansion of leveling rods, and scale errors of rod graduations (before 1980, rods were calibrated by using a microscope at 100-mm intervals; since then rods have been calibrated at every 5-mm graduation by a laser interferometer at the National Institute of Standards and Technology). Atmospheric refraction error is dependent upon the vertical temperature gradient along the line of sight. The gradient was not measured before 1980, and so it was predicted for the pre-1980 surveys by using the solar radiation model of *Holdahl* [1981]. We estimate the residual rod error for the preseismic surveys to be ± 20 ppm $\times$ dH after correction [*Stein*, 1981], where dH is the height difference from the endpoint bench mark, and 40 ppm $\times$ dH for residual refraction error. The residual refraction error assumes a 50% error in our estimate of the temperature gradient [*Stein et al.*, 1986], which gives a rms residual error for the coseismic period of about 8 mm.

Subsidence Corrections

Though smaller than the coseismic or postseismic deformation, artificial subsidence caused by fluid withdrawal [*Bull*, 1975; *Poland et al.*, 1975; *Ireland et al.*, 1982] must be removed to isolate tectonic elevation changes. We use the subsidence rate measured during 1966–1972 to correct the coseismic (1972–1983) deformation, modified by changes in the rate of subsidence after 1972 (Figure A1*b*). These modifications reflect the record of oil and groundwater withdrawal, compaction of the uppermost 300–700 m of sediments, water deliveries from the California aqueduct, and elevation changes with respect to more stable bench marks in consolidated Miocene marine sedimentary rocks 20 km northwest and 40 km southwest of the Coalinga epicenter. We identify leveling segments in Figure 5, and list the correction scheme in Table A3 and the corrected observations in Table A2.

San Joaquin Valley. Subsidence caused by water table decline at the western margin of the San Joaquin Valley reached a peak during the mid-1950s and largely abated after

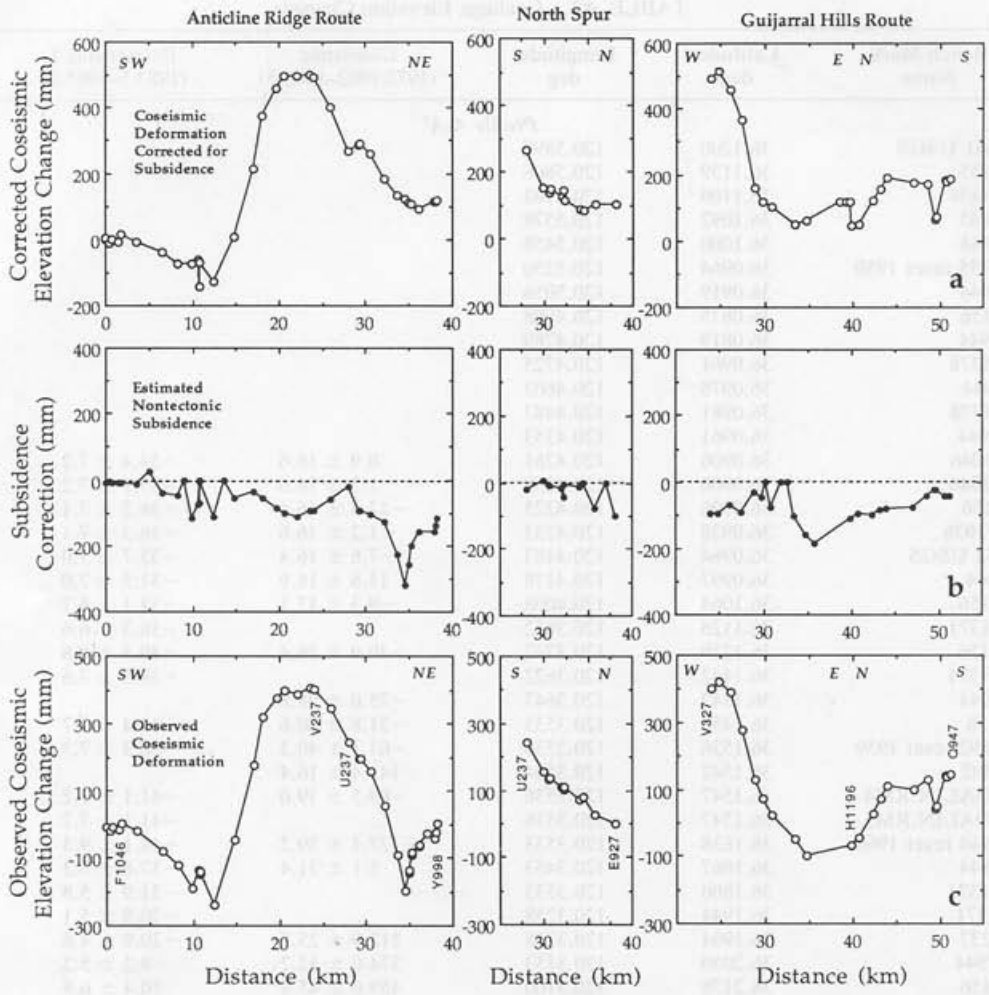

Fig. A1. Profiles of (*a*) subsidence-corrected coseismic elevation changes, (*b*) subsidence correction, and (*c*) observed coseismic (1969/1982–1983) elevation changes, along three leveling routes. Anticline Ridge route is along profile A–A′; endpoint bench marks of all routes located in Figure 5.

1970, when importation of California aqueduct water replaced pumping from deep aquifers [*Bull*, 1975]. During 1970–1983, the aqueduct delivered 93% of the water used for irrigation [*Ireland et al.*, 1982; *Ireland*, 1986]. Thus the subsidence rate observed during 1966–1972 is higher than that for the subsequent decade. Deep-well compaction recorders measured the compression of surface deposits in the most intensively pumped aquifers [*Poland et al.*, 1975; *Ireland*, 1986]. Compaction well 18S/16E-33A1 ("33A1," Figure 5; 313 m deep) recorded 275 mm of compaction during the period March 1966 to February 1982. CDWR leveling during this period from bench mark Y 998 at the well to bedrock sites at Anticline Ridge (V 237), Cantua Creek (U 928), and Kettleman Hills South Dome (D 666) shows 300 mm of subsidence, indicating that most compaction occurs at depths <300 m and is recorded by the compaction well. The rate of well compaction during 1972–1983 was 30% of the rate during 1966–1972; the rate was steady during 1978–1984.

Compaction well 19S/16E-23P2 ("23P2," Figure 5; 670 m deep) operated through 1974. During 1966–1972, the well recorded 100% of the subsidence measured by releveling to nearby bench mark Z 888 (Figure 5). During the next 2 years, the compaction rate declined 60%. The aquifer continued to recharge after 1974 [*Ireland*, 1986], so the expected 1972–1983 rate should also be about 30% of the 1966–1972 rate, or about 4.3 mm yr^{-1} (Table A3). Because the CDWR surveyed the northeast end of line A–A′ in 1982, the subsidence correction for 1982–1983 along the main leveling route is small.

Pleasant Valley. During 1960–1968, the rate of subsidence in Pleasant Valley was one-third the rate in the San Joaquin Valley [*Propokovitch and Magleby*, 1968]. After 1972, subsidence in Pleasant Valley is less certain because it was not resurveyed until 1983, and no compaction-recorder wells were sited there. We therefore use several indirect estimates of subsidence: Aqueduct deliveries to Coalinga township, in the center of the Pleasant valley, increased from 2% of the total water consumed in 1970–1971 to 30% of the total during 1972–1982 (Bureau of Reclamation, unpublished water delivery records, 1983). Estimated groundwater pumpage decreased by 40% from 1966–1972 to 1975–1977 (for T.20 S./R.15 E [*Mitten*, 1972, 1976, 1980]). Although no pumping records are available for 1972–1974 and 1978–1983,

TABLE A2. Coalinga Elevation Changes

Bench Mark	Bench Mark Name	Latitude, deg	Longitude, deg	Coseismic (1972/1982–1983.5)	Postseismic I (1983.5–1985.2)	Postseismic II (1985.2–1987.6)
			Profile A-A'			
1	1661 USGS	36.1200	120.5897			0.0 ± 11.9
2	V155	36.1139	120.5806			0.5 ± 11.7
3	B9454	36.1100	120.5703			−10.2 ± 11.6
4	A945	36.1092	120.5578			−3.1 ± 11.4
5	Z944	36.1000	120.5458			−5.4 ± 11.2
6	X155 reset 1950	36.0964	120.5250			−8.9 ± 10.9
7	R944	36.0919	120.5056			−6.2 ± 10.6
8	C156	36.0875	120.4908			−4.8 ± 10.4
9	Q944	36.0819	120.4789			−2.8 ± 10.2
10	C1378	36.0961	120.4725			1.1 ± 9.8
11	P944	36.0978	120.4603			−2.2 ± 9.6
12	B1378	36.0981	120.4483			4.2 ± 9.4
13	K944	36.0961	120.4353			4.0 ± 9.1
14	F1046	36.0906	120.4261	0.9 ± 16.6	−34.4 ± 7.2	2.9 ± 8.9
15	E1046	36.0906	120.4258	1.3 ± 16.6	−35.1 ± 7.2	3.5 ± 8.9
16	F156	36.0906	120.4225	−12.8 ± 16.4	−36.2 ± 7.1	2.3 ± 8.8
17	W1036	36.0928	120.4233	−1.2 ± 16.6	−36.3 ± 7.1	3.7 ± 8.8
18	852 USGS	36.0964	120.4183	−7.6 ± 16.4	−35.7 ± 7.0	−0.5 ± 8.6
19	J944	36.0997	120.4178	13.8 ± 16.9	−31.5 ± 7.0	−12.7 ± 8.6
20	G156	36.1064	120.4008	−9.3 ± 17.1	−33.1 ± 6.7	3.1 ± 8.3
21	G1371	36.1128	120.3872		−36.3 ± 6.6	−1.4 ± 8.2
22	H156	36.1219	120.3742	−40.9 ± 26.4	−40.4 ± 6.8	−2.7 ± 8.6
23	K1371	36.1442	120.3622		−38.3 ± 7.6	10.2 ± 9.8
24	G944	36.1342	120.3647	−75.0 ± 28.8		
25	J156	36.1458	120.3533	−31.8 ± 60.6	−44.4 ± 9.7	1.9 ± 12.9
26	Y692 reset 1959	36.1536	120.3536	−63.1 ± 40.3	−38.3 ± 7.3	5.8 ± 9.5
27	Z692	36.1542	120.3544	−141.4 ± 16.4		
28	COALIN.RM4	36.1547	120.3536	−69.5 ± 39.0	−41.1 ± 7.2	6.5 ± 9.3
29	COALIN.RM5	36.1547	120.3536		−41.1 ± 7.7	7.2 ± 10.0
30	X944 reset 1966	36.1638	120.3533	−127.1 ± 59.2	−44.1 ± 9.3	12.1 ± 12.4
31	Y944	36.1867	120.3453	5.1 ± 31.4	−37.6 ± 7.3	16.0 ± 7.5
32	H1371	36.1800	120.3533		−31.9 ± 5.8	17.2 ± 9.5
33	J1371	36.1944	120.3258		−20.9 ± 5.1	22.5 ± 6.6
34	X237	36.1994	120.3258	212.9 ± 25.5	−20.9 ± 4.6	22.0 ± 5.9
35	W944	36.2050	120.3153	374.0 ± 32.2	−9.2 ± 5.3	27.2 ± 6.9
36	V156	36.2178	120.3100	459.6 ± 45.9	10.4 ± 6.9	38.5 ± 9.3
37	V944	36.2253	120.3131	497.6 ± 52.5	9.4 ± 7.2	38.2 ± 9.8
38	W156	36.2392	120.3136	498.4 ± 58.2	17.9 ± 8.0	51.1 ± 10.8
39	V928	36.2444	120.3172	506.0 ± 49.6	18.1 ± 6.6	44.4 ± 9.0
40	V237 reset 1956	36.2467	120.3144	494.7 ± 49.6	11.1 ± 6.5	49.4 ± 8.9
41	H1228	36.2633	120.3106	402.4 ± 33.1	10.6 ± 8.4	39.4 ± 19.5
42	U237	36.2786	120.3014	265.5 ± 19.4	23.5 ± 3.3	24.0 ± 4.2
43	E929	36.2833	120.2958	286.9 ± 16.0	15.7 ± 3.4	27.6 ± 4.3
44	V692	36.2825	120.2956	290.1 ± 16.0	16.0 ± 3.4	27.4 ± 4.3
45	U692	36.2775	120.2831	259.1 ± 16.0	10.0 ± 3.8	21.5 ± 4.8
46	T692	36.2850	120.2703	180.2 ± 16.0	−8.0 ± 4.4	9.5 ± 5.5
47	M1371	36.2925	120.2700		0.2 ± 5.6	13.1 ± 7.2
48	S692	36.2978	120.2642	126.2 ± 16.5	−9.8 ± 7.1	10.3 ± 9.4
49	P805	36.3031	120.2581	108.4 ± 17.1	−7.0 ± 9.7	22.8 ± 12.9
50	H882	36.3061	120.2539	104.1 ± 16.6	−12.5 ± 7.0	21.0 ± 9.2
51	R692	36.3083	120.2517	103.0 ± 16.2	−20.3 ± 5.3	5.1 ± 6.7
52	PV3 BOR	36.3083	120.2511		−13.2 ± 5.2	12.2 ± 6.6
53	PV4 BOR	36.3061	120.2539		−9.2 ± 5.2	
54	PV2 BOR	36.3144	120.2442		−18.3 ± 5.1	2.7 ± 6.6
55	PV1 BOR	36.3197	120.2375		−16.5 ± 5.2	3.0 ± 7.5
56	E885	36.3139	120.2453	92.7 ± 16.0	−12.4 ± 5.9	2.4 ± 6.3
57	143.12R BOR	36.3267	120.2303	122.4 ± 16.5	−14.3 ± 7.5	3.2 ± 9.8
58	143.12L BOR	36.3267	120.2300	126.1 ± 17.1	−17.6 ± 9.3	−1.2 ± 12.3
59	Y998 USGS	36.3267	120.2289	129.0 ± 17.3	−18.0 ± 10.4	−4.8 ± 13.8
60	R1195	36.3269	120.2358	125.6 ± 16.6	−12.2 ± 8.1	4.8 ± 10.6
61	X1074	36.3308	120.2403	132.1 ± 17.5	−17.1 ± 11.1	3.2 ± 14.8
62	Q1195	36.3353	120.2417	131.4 ± 17.7	−19.4 ± 11.1	−8.4 ± 15.8
			Profile B-B'			
63	Y662	36.2967	120.3011	151.7 ± 16.1		
64	R984	36.3014	120.3014	137.3 ± 16.3		
65	P929	36.3017	120.3003	145.3 ± 16.5		
66	T237	36.3117	120.3036	123.7 ± 17.9		
67	C984	36.3131	120.3033	142.9 ± 26.4		
68	B984	36.3139	120.3036	108.0 ± 16.3		

TABLE A2. (continued)

Bench Mark	Bench Mark Name	Latitude, deg	Longitude, deg	Coseismic (1972/1982–1983.5)	Postseismic I (1983.5–1985.2)	Postseismic II (1985.2–1987.6)
			Profile B-B'(continued)			
69	X662	36.3269	120.3003	85.0 ± 17.7		
70	U1195	36.3311	120.2978	82.9 ± 16.0		
71	B1196	36.3417	120.3011	76.2 ± 16.5		
72	E927	36.3561	120.3192	101.1 ± 52.5		
73	J929	36.2494	120.3078	517.0 ± 50.1		
74	X156	36.2486	120.2925	459.0 ± 38.5		
75	G929	36.2497	120.2778	366.0 ± 47.8		
76	Y156	36.2542	120.2628	159.0 ± 21.9		
77	5.88L BOR	36.2544	120.2528	116.5 ± 27.6		
78	T1096	36.2542	120.2425	88.9 ± 42.1		
79	H927	36.2539	120.2133	50.7 ± 59.2		
80	G1196	36.2456	120.2092	51.1 ± 81.1		
			Profile C-B			
81	H1196	36.2025	120.2108	43.5 ± 57.3		
82	K512	36.1953	120.2092	48.0 ± 49.6		
83	H512 reset 1964	36.1811	120.2092	113.3 ± 51.5		
84	Phelps Az Mk	36.1733	120.2092	150.1 ± 44.9		
85	T228	36.1664	120.2100	182.3 ± 43.1		
86	F512	36.1383	120.2100	169.3 ± 40.8		
87	D512	36.1372	120.2261	164.6 ± 25.6		
88	GUIJARRAL	36.1511	120.2339	161.0 ± 23.0		
89	GUJAR.RMI	36.1514	120.2342	162.1 ± 23.0		
90	P947	36.1503	120.2353	160.3 ± 23.0		
91	Q947	36.1492	120.2389	166.8 ± 23.0		

Profiles refer to leveling route segments in Figure 5; certainties quoted. A constant can be freely added to all data.

TABLE A3. Coalinga Coseismic Subsidence Correction

Leveling Segment (Keyed to Figure 5)	Number of Bench Marks	Coseismic Period, Years	SubsidenceRate Used	Mean Subsidence Rate, mm yr^{-1}	Mean Correction, mm
a, Pleasant Valley	17	1972–1985	0.5 × 1966–1972	3.4	44
b, Anticline Ridge (N and S)	17	1972–1985	1.0 × 1966–1972	4.0	52
c, Anticline Ridge (central)	6	1982–1985	0.5 × 1972–1982	7.0	21
d, San Joaquin Valley (N and S)	14	1972–1985	0.3 × 1966–1972	4.3	56
e, San Joaquin Valley (central)	11	1982–1985	1.0 × 1978–1982	3.0	9

The subsidence rate for five out of the 70 MBs was interpolated from adjacent BMs.

continued water table decline increased the cost of pumping, which probably reduced pumpage after 1977. Therefore, we assume that the subsidence rate for 1972–1983 was about 50% of the measured 1966–1972 rate, yielding a mean of 3.4 mm yr^{-1}.

Anticline Ridge. The net liquid production rate in the Coalinga and East Extension oil fields beneath Anticline Ridge (oil and water out less reinjected water and steam) has declined slightly since 1966, from 4.6 to 4.1 × 10^6 m^3 yr^{-1} (29 to 26 × 10^6 barrels yr^{-1} [see California Division of Oil and Gas, 1961; *Conservation Committee of California Oil Producers*, 1967–1984]). We therefore use the 1966–1972 subsidence rate, 5.5 mm yr^{-1}, to correct the coseismic elevation changes. The CDWR surveyed the east half of the anticline in 1982, and so the subsidence correction there is small. *Segall* [1985], who modeled the stress and elevation changes caused by fluid withdrawal beneath Anticline Ridge, predicted a near-linear subsidence rate of 3.3 ± 0.7 mm yr^{-1}, in fair agreement with the observed rate.

Acknowledgments. Jerry Eaton and Donna Eberhart-Phillips offered immeasurable help in interpreting seismograms and using the three-dimensional velocity model, for which we are grateful. We also thank David Oppenheimer for guiding us through the labyrinth of Calnet, Tousson Toppozada for directing us to the 1885 earthquake, Geoffrey King for introducing us to his boundary element program, Ken Hudnut, Ron Bruhn, Wayne Thatcher, Bob Simpson, and an anonymous referee for their thoughtful reviews. G.E. was supported by the U.S. Geological Survey and by the National Science Foundation grant EAR 88-03786.

REFERENCES

Atwater, B. F., D. A. Trumm, J. C. Tinsley, R. S. Stein, A. B. Tucker, D. J. Donahue, A. J. T. Jull, and L. A. Payen, Alluvial plains and earthquake recurrence at the Coalinga anticline, in The Coalinga, California Earthquake of May 2, 1983, edited by M. Rymer and W. Ellsworth, *U.S. Geol. Surv. Prof. Pap., 1487*, 273–297, 1990.

Bull, W. B., Land subsidence due to ground-water withdrawal in the Los Baños-Kettleman City area, California, 2, Subsidence and

compaction of deposits, *U.S. Geol. Surv. Prof. Pap., 437-F*, 89 pp., 1975.

Byerly, P., The Idria (California) earthquake of July 25, 1926, *Bull. Seismol. Soc. Am., 17*, 203–206, 1927.

California Division of Oil and Gas, California oil and gas fields, maps and data sheets, San Francisco, 1961.

Choy, G. L., Source parameters of the earthquake, as inferred from broadband body waves, in The Coalinga, California Earthquake of May 2, 1983, edited by M. Rymer and W. Ellsworth, *U.S. Geol. Surv. Prof. Pap., 1487*, 193–205, 1990.

Conservation Committee of California Oil Producers, Annual review of California oil and gas production, Los Angeles, 1967–1984.

Davis, T. L., J. Namson, and R. F. Yerkes, A cross section of the Los Angeles area: Seismically active fold and thrust belt, the 1987 Whittier Narrows earthquake, and earthquake hazard, *J. Geophys. Res., 94*, 9644–9664, 1989.

DeMets, C., R. G. Gordon, D. F. Argus, and S. Stein, Current plate motions, *Geophys. J. Int., 101*, 425–478, 1990.

Eaton, J. P., The earthquake and its aftershocks from May 2 through September 30, 1983, in The Coalinga, California Earthquake of May 2, 1983, edited by M. Rymer and W. Ellsworth, *U.S. Geol. Surv. Prof. Pap., 1487*, 113–170, 1990.

Eaton, J. P., and M. J. Rymer, Regional seismotectonic model for the southern Coast Ranges, in The Coalinga, California Earthquake of May 2, 1983, edited by M. Rymer and W. Ellsworth, *U.S. Geol. Surv. Prof. Pap., 1487*, 97–111, 1990.

Eaton, J. P., R. Cockerham, and F. Lester, Study of the May 2, 1983 Coalinga earthquake and its aftershocks, based on the USGS seismic network in northern California, in The 1983 Coalinga, California Earthquake, *Spec. Publ. Calif. Div. Mines Geol., 66*, 261–273, 1983.

Eberhart-Phillips, D., Active faulting and deformation of the Coalinga anticline from three-dimensional velocity structure and seismicity, *J. Geophys. Res., 94*, 15,565–15,586, 1989.

Eberhart-Phillips, D., Three-dimensional *P* and *S* velocity structure in the Coalinga region, California, *J. Geophys. Res., 95*, 15,343–15,364, 1990.

Ekström, G., and A. M. Dziewonski, Centroid-moment tensor solutions for 35 earthquakes in western North America (1977–1983), *Bull. Seismol. Soc. Am., 75*, 23–39, 1985.

Ekström, G., R. S. Stein, J. P. Eaton, and D. Eberhart-Phillips, Seismicity and geometry of a 100-km-long blind thrust fault, 1, The 1985 Kettleman Hills, California, Earthquake, *J. Geophys. Res.*, this issue.

Federal Geodetic Control Committee, *Standards and Specifications for Geodetic Control Networks*, National Geodetic Survey, Rockville, Md., 1984.

Hauksson, E., and L. M. Jones, The 1987 Whittier Narrows earthquake sequence in Los Angeles, southern California: Seismological and tectonic analysis, *J. Geophys. Res., 94*, 9569–9589, 1989.

Holdahl, S. R., A model of temperature stratification for correction of leveling refraction, *Bull. Geod., 55*, 231–249, 1981.

Ireland, R. L., Land subsidence in the San Joaquin Valley, California as of 1983, *U.S. Geol. Surv. Open File Rep., 85-4196*, 1986.

Ireland, R. L., J. F. Poland, and F. S. Riley, Land subsidence in the San Joaquin Valley, California as of 1980, *U.S. Geol. Surv. Open File Rep., 82-370*, 129 pp., 1982.

King, G. C. P., and M. Ellis, The origin of large local uplift in extensional regions, *Nature, 348*, 689–693, 1991.

Lin, J., and R. S. Stein, Coseismic folding, earthquake recurrence, and the 1987 source mechanism at Whittier Narrows, Los Angeles basin, California, *J. Geophys. Res., 94*, 9614–9632, 1989.

Medwedeff, D. A., Growth fault-bend folding at southeast Lost Hills, San Joaquin Valley, California, *AAPG Bull., 73*, 54–67, 1989.

Meltzer, A., Crustal structure and tectonic evolution: Central California, Ph.D. dissertation, pp. 95–167, Rice Univ., Houston, Tex., 1989.

Mitten, H. T., Ground-water pumpage, San Joaquin Valley, California, 1967–68, *U.S. Geol. Surv. Open File Rep.*, 1972.

Mitten, H. T., Estimated agricultural ground-water pumpage in parts of the San Joaquin Valley, California, 1969–71, *U.S. Geol. Surv. Open File Rep.*, 7 pp., 1976.

Mitten, H. T., Estimated agricultural ground-water pumpage in parts of the San Joaquin Valley, California, 1975–77, *U.S. Geol. Surv. Open File Rep., 80-1281*, 11 pp., 1980.

Mogi, A., B. Kawamura, and Y. Iwabuchi, Submarine crustal movement due to the Niigata earthquake in 1964, in the environs of Awa Sima Island, Japan Sea, *J. Geod. Soc. Jpn., 10*, 180–186, 1964.

Namson, J. S., and T. L. Davis, Seismically active fold and thrust belt in the San Joaquin Valley, central California, *Geol. Soc. Am. Bull., 100*, 257–273, 1988.

Namson, J. S., T. L. Davis, and M. B. Lagoe, Tectonic history and thrust-fold deformation style of seismically active structures near Coalinga, in the Coalinga, California Earthquake of May 2, 1983, edited by M. Rymer and W. Ellsworth, *U.S. Geol. Surv. Prof. Pap., 1487*, 79–96, 1990.

Poland, J. F., B. E. Lofgren, and R. L. Ireland, Land subsidence in the San Joaquin Valley, California, as of 1972, *U.S. Geol. Surv. Prof. Pap., 437-H*, 78 pp., 1975.

Prokopovitch, N. P., and D. C. Magelby, Land subsidence in Pleasant Valley, *J. Am. Water Works Assoc., 60*, 413–424, 1968.

Reches, Z., and M. D. Zoback, Theoretical analysis of the deformation of a layered sequence above a fault—Preliminary application to the Loma Prieta earthquake, in *Stanford Rock Physics and Borehole Geophysics*, vol. 40, X1–X22, Stanford University, Stanford, Calif., 1990.

Richter, C. F., *Elementary Seismology*, W. H. Freeman, New York, 1958.

Rodgers, D. A., and W. D. Rizer, Deformation and secondary faulting near the leading edge of a thrust fault, in *Thrust and Nappe Tectonics*, edited by K. R. McClay and N. J. Price, pp. 65–77, Geological Society of London, Oxford, England, 1981.

Rymer, M. J., K. J. Kendrick, J. J. Lienkaemper, and M. M. Clark, The Nuñez fault and its surface rupture during the Coalinga earthquake sequence, in The Coalinga, California Earthquake of May 2, 1983, edited by M. Rymer and W. Ellsworth, *U.S. Geol. Surv. Prof. Pap., 1487*, 299–318, 1990.

Satake, K., and K. Abe, A fault model for the Niigata, Japan, earthquake of June 16, 1964, *J. Phys. Earth, 31*, 217–223, 1983.

Scofield, C. P., W. H. Bakun, and A. G. Lindh, The 1982 New Idria, California earthquake sequence, in Mechanics of the Coalinga Earthquake, *U.S. Geol. Surv. Open File Rep., 85-44*, 403–429, 1985.

Segall, P., Stress and subsidence resulting from subsurface fluid withdrawal in the epicentral region of the 1983 Coalinga earthquake, *J. Geophys. Res., 90*, 6801–6816, 1985.

Sieh, K. E., and R. Jahns, Holocene activity of the San Andreas fault at Wallace Creek, California, *Geol. Soc. Am. Bull., 95*, 883–896, 1984.

Simpson, R. W., S. S. Schulz, L. D. Dietz, and R. O. Burford, The response of creeping parts of the San Andreas fault to earthquakes on nearby faults—Two examples, *Pure Appl. Geophys., 126*, 665–685, 1988.

Sipkin, S. A., and R. L. Needham, Kinematic source parameters determined by time-dependent moment-tensor inversion and an analysis of teleseismic first motions, *U.S. Geol. Surv. Prof. Pap., 1487*, 207–214, 1990.

Stein, R. S., Discrimination of tectonic displacement from slope-dependent errors in geodetic leveling from southern California, 1953–1979, in *Earthquake Prediction: An International Review, Maurice Ewing Ser.*, vol. 4, edited by D. W. Simpson and P. G. Richards, pp. 441–456, AGU, Washington, D. C., 1981.

Stein, R. S., and G. C. P. King, Seismic potential revealed by surface folding: 1983 Coalinga, California, earthquake, *Science, 224*, 869–872, 1984.

Stein, R. S., and R. S. Yeats, Hidden Earthquakes, *Sci. Am., 260* (6), 48–57, 1989.

Stein, R. S., C. T. Whalen, S. R. Holdahl, W. E. Strange, and W. Thatcher, Saugus-Palmdale field test for refraction error in historical leveling surveys, *J. Geophys. Res., 91*, 9031–9044, 1986.

Stein, R. S., C. T. Whalen, S. R. Holdahl, W. E. Strange, and W. Thatcher, Reply, *J. Geophys. Res., 92*, 10,715–10,717, 1987.

Stein, R. S., C. T. Whalen, S. R. Holdahl, W. E. Strange, and W. Thatcher, Reply to "Comment on 'Saugus-Palmdale, California, field test for refraction error in historical leveling surveys,' by R. S. Stein, C. T. Whalen, S. R. Holdahl, W. Strange, and W. Thatcher" and Comment on "Further analysis of the 1981 south-

ern California field test for leveling refraction," by M. R. Craymer and P. Vanicek, *J. Geophys. Res.*, *94*, 7673–7677, 1989.

Stover, C. W., Intensity distribution and isoseismal map, in The 1983 Coalinga, California Earthquake, California, *Spec. Publ. Calif. Div. Mines Geol.*, *66*, 1–4, 1983.

Stover, C. W., and L. R. Brewer, United States earthquakes, 1985, *U.S. Geol. Surv. Bull.*, *1954*, 170 pp., 1991.

Suppe, J., Geometry and kinematics of fault-bend folding, *Am. J. Sci.*, *283*, 684–721, 1983.

Toppozada, T. R., D. L. Parke, and C. T. Higgins, Seismicity of California 1900–1931, *Spec. Rep. Calif. Div. Mines Geol.*, *135*, 135 pp., 1978.

Toppozada, T. R., C. R. Real, and D. L. Parke, Preparation of isoseismal maps and summaries of reported effects for pre-1900 California earthquakes, *Calif. Div. Mines Geol. Open File Rep.*, *81-11 SAC*, 182 pp., 1981.

Toppozada, T. R., C. Hallstrom, and D. Ransom, $M \geq 5.5$ earthquakes within 100 km of Parkfield, CA, *Seismol. Res. Lett.*, *61*, 42, 1990.

Townley, S. D., and M. W. Allen, Descriptive catalog of earthquakes of the Pacific coast of the United States 1769 to 1928, *Bull. Seismol. Soc. Am.*, *29*, 1–297, 1939.

Wentworth, C. M., and M. D. Zoback, The style of late Cenozoic deformation at the eastern front of the California Coast ranges, *Tectonics*, *8*, 237–246, 1989.

Wesson, R. L., and C. Nicholson, Intermediate-term, pre-earthquake phenomena in California, 1975–86, and preliminary forecast of seismicity for the next decade, *Pure Appl. Geophys.*, *126*, 407–446, 1988.

Wetmiller, R. J., R. B. Horner, H. S. Hasegawa, R. G. North, M. Lamontagne, D. H. Weichert, and S. G. Evans, An analysis of the 1985 Nahanni earthquakes, *Bull. Seismol. Soc. Am.*, *78*, 590–616, 1988.

Yeats, R. S., G. J. Huftile, and F. B. Grigsby, Oak Ridge fault, Ventura fold belt, and the Sisar decollement, Ventura basin, California, *Geology*, *16*, 1112–1116, 1988.

Yerkes, R. F., P. Levine, and C. M. Wentworth, Abnormally high fluid pressures in the region of the Coalinga earthquake sequence and their significance, in The Coalinga, California Earthquake of May 2, 1983, edited by M. Rymer and W. Ellsworth, *U.S. Geol. Surv. Prof. Pap.*, *1487*, 235–257, 1990.

Zigler, J. L. C. M. Wentworth, and J. A. Bartow, Structure contour map of the tops of the Kreyenhagen formation and Cretaceous strata in the Coalinga area, Fresno and Kings counties, California, *U.S. Geol. Surv. Misc. Field Stud. Map, MF-1843*, 1986.

G. A. Ekström, Department of Earth & Planetary Sciences, Harvard University, 24 Oxford Street, Cambridge, MA 02138 (Tel. 617-496-8276; Fax 617-495-8839).

R. S. Stein, U.S. Geological Survey, 345 Middlefield Road, MS 977, Menlo Park, CA 94025 (Tel. 415-329-4840; Fax 415-329-5163).

(Received October 17, 1990;
revised October 15, 1991;
accepted November 8, 1991.)